Journal of Geosciences, 59 (2014), 183–208 DOI: 10.3190/jgeosci.174

Original paper

Architecture of thrust faults with alongstrike variations in fault-plane dip: anatomy of the Lusatian Fault, Bohemian Massif

Miroslav COUBAL[1]*, Jiří ADAMOVIČ[1], Jiří MÁLEK[2], Vladimír PROUZA[3]

[1] *Institute of Geology, v.v.i., Academy of Sciences of the Czech Republic, Rozvojová 269, 165 00 Prague 6, Czech Republic; coubal@gli.cas.cz*

[2] *Institute of Rock Structure and Mechanics, v.v.i., Academy of Sciences of the Czech Republic, V Holešovičkách 41, 182 09 Prague 8, Czech Republic*

[3] *Czech Geological Survey, Klárov 3/131, 118 21 Prague 1, Czech Republic*

* *Corresponding author*

The Lusatian Fault in the northern Bohemian Massif is one of the most prominent products of the latest Cretaceous to Paleogene thrusting in the Alpine foreland in Europe. Its fault plane dips to the N to NE, typically separating crystalline units in the N from Upper Paleozoic and Cretaceous units in the south. Crystalline units in Lusatia consist of Proterozoic to Lower Paleozoic rocks epi- to mesozonally metamorphosed during the Variscan Orogeny, cut by Cadomian and Variscan granitoid plutons. Anatomy of the fault was studied in outcrops and in a series of test trenches, and the course of fault trace in complex topography was used to determine the dip of the fault. Based on a detailed analysis of brittle structures accompanying the main fault, the Lusatian Fault Belt can be further subdivided into the fault core, zone of wall-rock brecciation, and the damage zone which also includes large-scale dismembered blocks and flanking structures. Other components of the fault belt originated in spatial association with the Lusatian Fault, during its formation (e.g., the drag zone and bedding-plane slips in the footwall-block sediments) or later, during its multi-stage evolution.

A general dependence of fault belt architecture on the orientation of the fault plane to the acting stress can be demonstrated. With the NNE–SSW subhorizontal maximum principal stress calculated for the thrusting episode at the Lusatian Fault, less complex structures appear where the dip of the fault is shallower, and more complex structures including thicker damage zone and drag zone were formed where the fault was steeper. In flat fault segments, competent members of the footwall-block sedimentary package, whose bedding planes were sub-conformable to the fault plane, were sheared during the thrusting and dragged to near-surface levels as dismembered blocks. A progressive eastward increase in the fault dip angle is associated with the appearance of the zone of flanking structures in which the degree of rotation is a function of the fault dip angle. In the eastern part of the fault (fault dip angle of ~60°), the same stress acted at a high angle to the fault plane producing a "bulldozer effect". Limbs of the flanking structures were overturned, and a parallel, more gently inclined Frýdštejn Fault was initiated as a structure more advantageous for slip movement.

Keywords: fault architecture, fault plane geometry, drag structures, thrust fault, sandstone, Lusatian Fault
Received: 8 August 2013; accepted: 24 June 2014; handling editor: J. Žák

1. Introduction

The Alpine tectonic evolution of the Elbe Fault System, initiated during the Variscan Orogeny and traversing a large part of Europe between the North Sea and the Sudetes (Fig. 1), has been recently reviewed by many papers, e.g., Ziegler (1987), Scheck et al. (2002), Ziegler and Dèzes (2007), and Kley and Voigt (2008). These papers helped to describe crustal structure in this region and explained the general kinematics of this system and its geodynamic causes. However, only two fault segments have been subjected to a detailed analysis of fault geometry and kinematics and to paleostress analysis: the Northern Harz Border Fault (Franzke et al. 2004) and the Teisseyre–Tornquist Zone (Bergerat et al. 2007).

The Lusatian Fault (LF) is a major deep-reaching structure of the Variscan Elbe Fault System (Fig. 1), which was activated as a thrust fault in the latest Cretaceous to Paleogene times, accommodating the uplift of the Sudetic Block and contributing to significant crustal shortening in the Alpine foreland (Bergerat 1987; Ziegler 1987). In the existing geological maps (e.g., Kozdrój et al. 2001), the LF is presented as a structure with a uniform deformation pattern along its strike. At a closer look, however, the situation is more complex, combining several structural components expressed to a different degree along the fault strike. The variety of structural elements observed with the multiphase kinematic character of the fault make the LF an ideal natural laboratory for examination of these structures and their mutual relationships.

The architecture of the middle and eastern segments of the Lusatian Fault Belt (LF Belt), i.e. complex of structures of different types concentrated to the neigh-

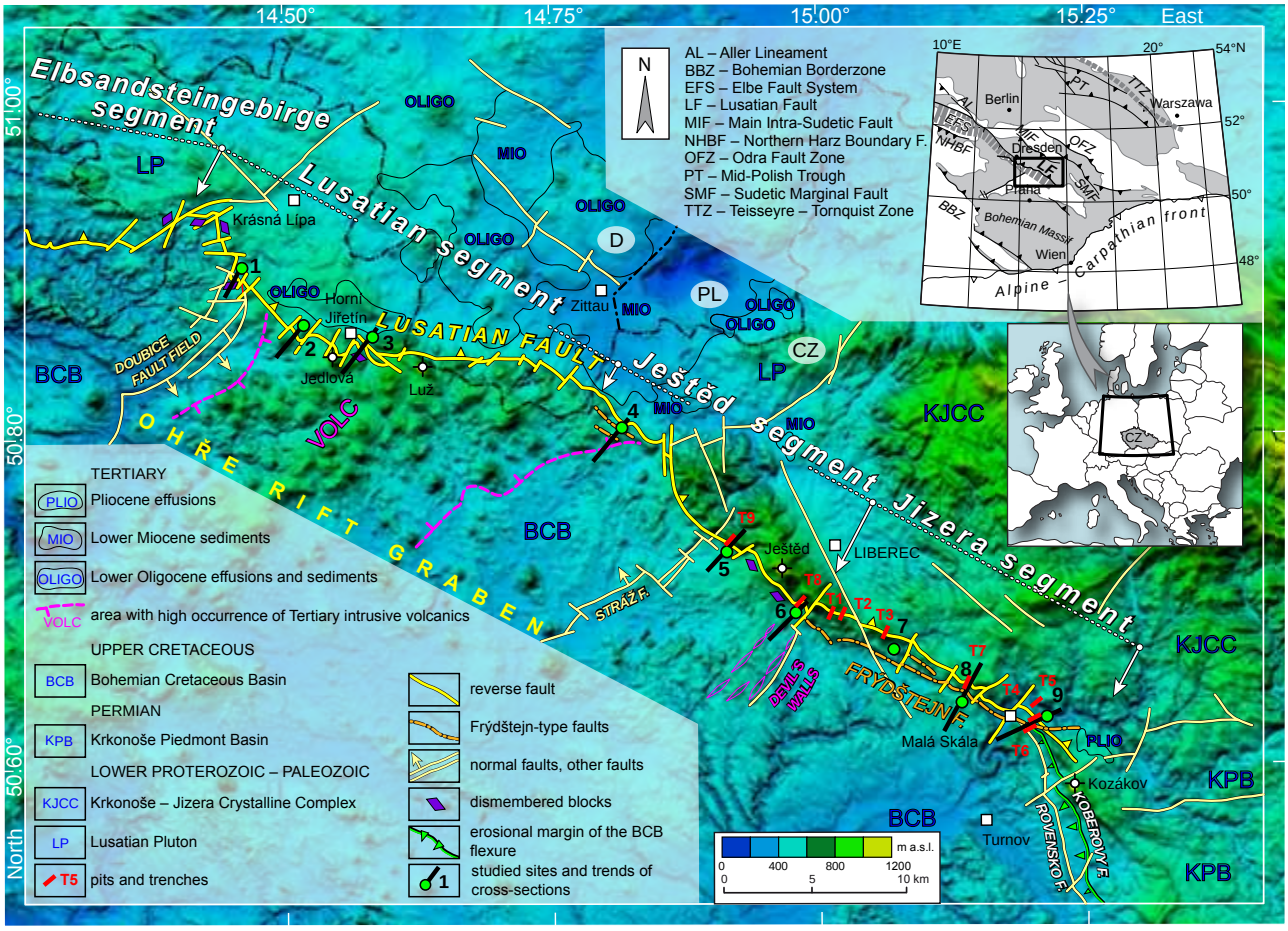

Fig. 1 A map showing the general course of the middle and eastern parts of the Lusatian Fault, locations of the studied sites and recently excavated test pits/trenches.

bourhood of the LF, was studied in detail along several key transects by the present authors (Fig. 1). Results of two decades of new research are presented in two steps. First, architecture of the fault belt is described. Second, a kinematic model is formulated for the origin of the Lusatian Fault backed by observations along transverse profiles, explaining the observed alongstrike variations in fault belt architecture. Our data demonstrate that this variation was controlled by contrasting dip angles of the fault plane even if the whole fault belt was activated by a homogeneous stress field. We suggest this mechanism to be of general validity in the evolution of fault belts.

2. Geological setting

The Lusatian Fault (LF) extends from Meissen, Saxony in the WNW to Kozákov Hill near Turnov, Bohemia in the ESE (Fig. 1). Its main fault plane dips approximately to the NNE (N to NE). In a general view, the LF separates the Neoproterozoic to Lower Paleozoic Krkonoše–Jizera Crystalline Complex and the Lusatian Pluton in the N from the sedimentary and volcanic rocks of the Late Paleozoic basins and the Bohemian Cretaceous Basin in the S (Fig. 1; Malkovský 1977, 1987). The relative position of the two wall blocks separated by the LF is compatible with reverse faulting showing a vertical displacement in excess of 1000 m. The real displacement is possibly much higher as suggested by the summary of apatite fission-track data from the granitic rocks of the Krkonoše Mts.: over *c.* 3.6 km could have been eroded from the hangingwall block of the LF since the Turonian (Migoń and Danišík 2012).

In spite of the very early interest in the prominent southern geological boundary of the Variscan crystalline complexes in Lusatia (Weiss 1827; Cotta 1838), modern literature on the structure of the later defined LF (Suess 1903) is insufficient, dealing only with certain fault segments or specific aspects of the fault belt. In Saxony, the course of the fault was documented by Wagenbreth (1966, 1967). Geometry of the fault plane in Bohemia is poorly known and, although the fault displays as a single moderately-dipping plane in the MVE-90 (East) reflection seismic profile (DEKORP-BASIN Research

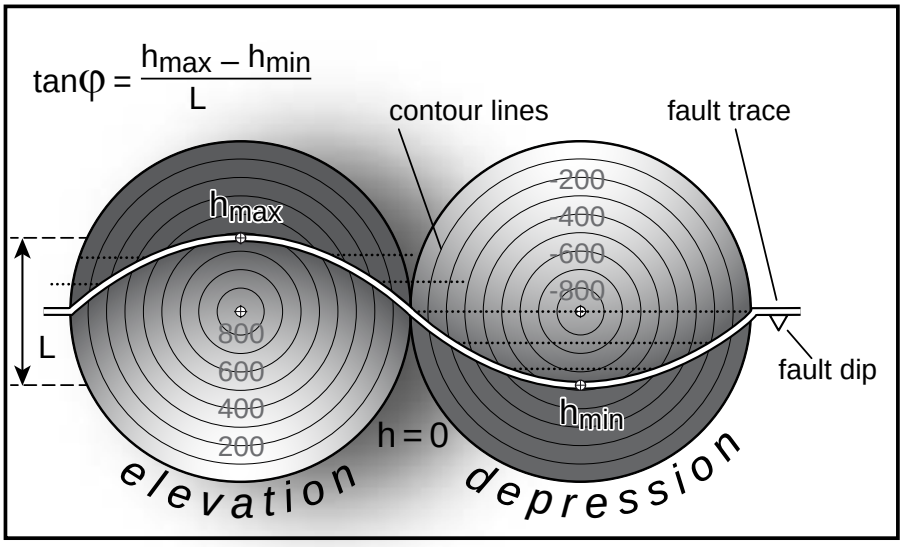

Fig. 2 Determination of the dip angle **φ** of the fault plane by the sigmoidal course of the fault trace in a complex relief. The course of the fault trace results from the intersection of an even, non-vertical fault plane with prominent landforms. A connection line between two intersections of a certain relief contour line with the fault trace represents a contour line of the fault plane. The strike and the dip angle of the fault plane are indicated by a set of contour lines thus constructed.

Group 1999), field evidence suggests the presence of parallel faults and rotated blocks of Cretaceous sediments in its footwall block (Krejčí 1869; Zahálka 1902; Coubal 1990). Existing data from crystalline rocks in the hangingwall block are scarce (e.g., Fediuk et al. 1958; Bělohradský and Petrin 1977; Reichmann 1979) and do not allow discriminating between deformations of different ages. The tectonic and kinematic history of the LF has been the subject of only general papers (e.g., Malkovský 1987).

Post-Cretaceous paleostress history of the LF area was studied by Coubal (1989, 1990) who provided the basic paleostress framework for the LF evolution. The group of latest Cretaceous to Paleogene compressional paleostress patterns **α** was identified to have governed the main thrusting process. Three paleostress patterns were specified by Adamovič and Coubal (1999), of which NE–SW-orientated subhorizontal compression $\boldsymbol{\alpha}_1$ was responsible for the origin of the fault belt. The fault belt was further modified by paleostress patterns $\boldsymbol{\alpha}_2$ (N–S compression) and $\boldsymbol{\alpha}_3$ (NNW–SSE compression).

3. Methods

The study of the internal structure of the LF Belt in Bohemia is based on nine cross sections parallel to the transport direction at the main fault (Fig. 1). Locations of the cross sections were chosen to represent all fault segments of different structural settings and to be well substantiated by data: outcrops and technical works (mostly boreholes) related to mineral prospection and/or mining (Fig. 1). Besides archival data, results from new test pits and trenches were taken into account. Test trenches T1–T9 were excavated by the present team along nine transects across the LF in 1997 and their descriptions have been hitherto contained only in the unpublished report of Prouza et al. (1999).

The best method used for the determination of the dip angle of the main fault plane was the detailed tracing of its course in the field. A moderately to gently dipping fault plane intersects the present uneven erosional surface in an arched trace, which allows to reconstruct the orientation of the fault plane much more precisely than from the results of a trenching survey (Fig. 2). Besides fault-trace mapping, fieldwork also included a routine measurement of orientations of brittle tectonic structures, mineralized zones, and the dips of strata. Other features were also documented in trenches T1–T9 and in natural outcrops along the fault. Among the routinely measured features of brittle structures, we exploited particularly those allowing the determination of the extent of the individual architectural elements of the fault. Results of the study of brittle structure kinematics, X-ray diffraction analyses and grain-size analyses of fault rocks of the LF core are only briefly mentioned.

4. Nomenclature of architectural elements of a fault

Most large faults exhibit a fault-parallel zoning in which individual architectural elements can be distinguished. Fault core is a central high-strain zone accommodating a large portion of fault movements and usually containing one or several principal slip zones. Various compositions of the core were presented (Shipton et al. 2006; Childs et al. 2009; Caine et al. 2010; Faulkner et al. 2010), ranging from a single layer of fault rocks to combinations of multiple fault-rock bodies and wall-rock lenses. Parts of the footwall and hangingwall blocks adjacent to the fault core can be transected by many types of subordinate structures

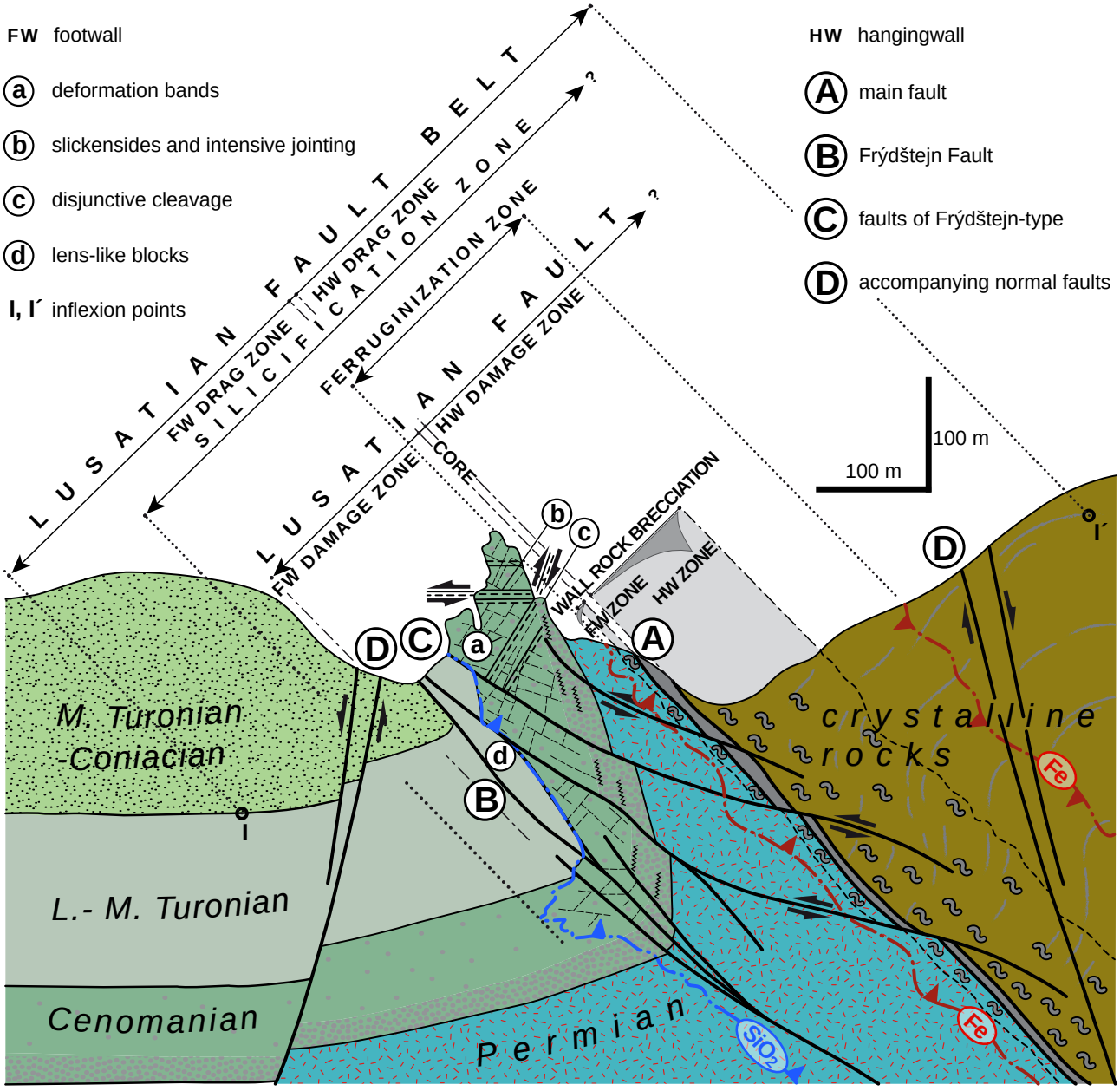

Fig. 3 An overview of the architectural elements of the Lusatian Fault Belt. A blue line 'SiO_2' marks the extent of silicification in the footwall block, red lines labelled 'Fe' delineate the ferruginization zone.

associated with the fault movement. Depending on their predominant brittle or ductile character, a damage zone or a drag zone are defined, respectively (Fossen 2010). A predominantly ductile behaviour produces a continuous deflection of planar elements in rock fabric termed flanking structures (e.g., Passchier 2001), while predominance of brittle structures accentuates the role of dismembered blocks in the fault belt. Bodies composed of breccia enter different fault architecture elements, typically the fault core or the membranes along its boundaries (Braathen et al. 2009) or the damage zone (Caine et al. 2010; Faulkner et al. 2010).

5. Anatomy of the Lusatian Fault/Fault Belt

5.1. Conceptual model

The main thrusting and the subsequent multiphase kinematic activity of the LF are reflected by the width and complexity of its fault belt. Based on the archival data and new field documentation, a conceptual model was constructed (Fig. 3). Quantitative characteristics of most of the architectural elements are discussed in Chapter 6 and Tables 1–2.

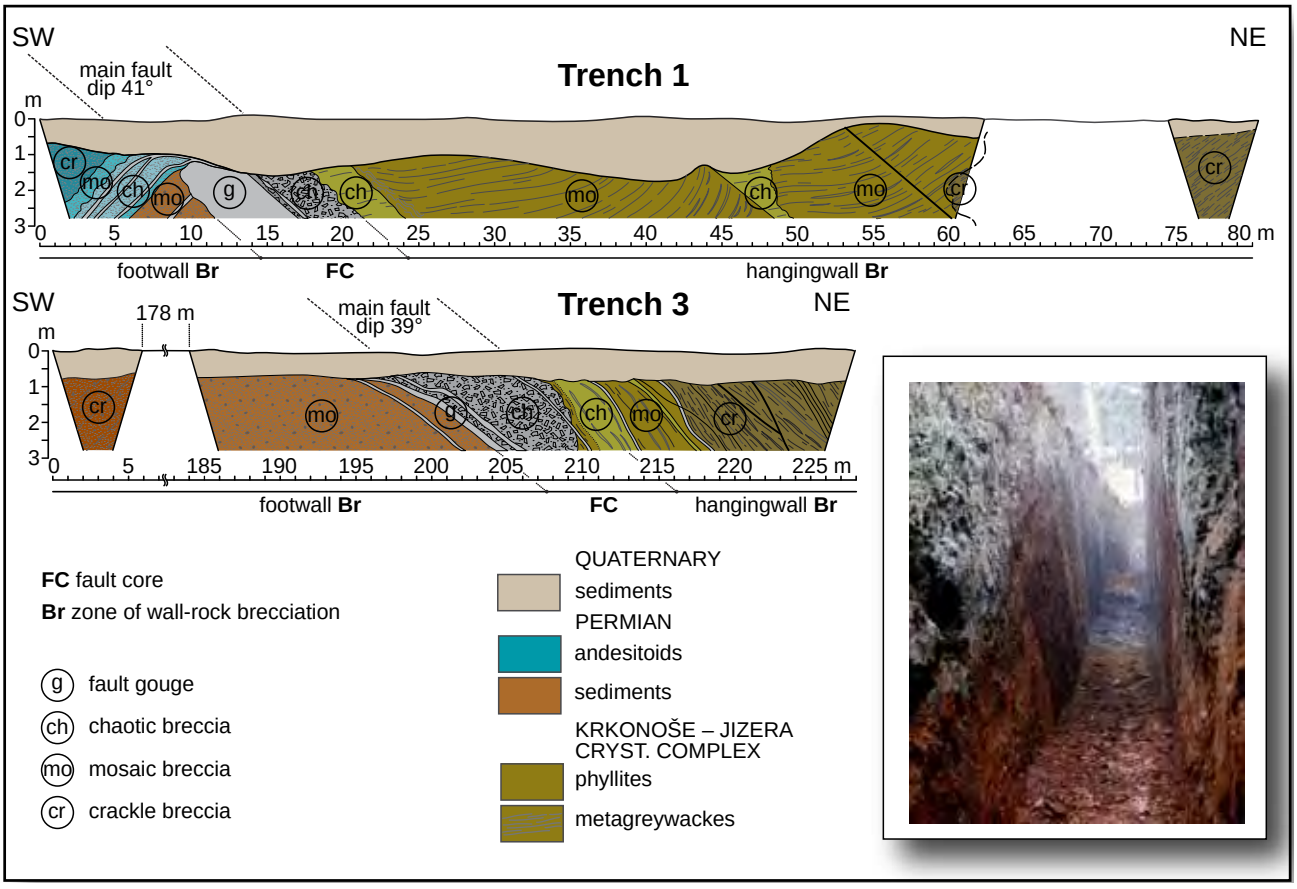

Fig. 4 Nature of the main fault and wall-rock brecciation, test trenches and pits T1 and T3 between sites 6 and 7. For locations see Fig. 1. Vertically exaggerated. Photo: Chaotic breccia in ferruginized chlorite–sericite phyllites (red) alternating with bands of mosaic breccia in silicified graphite phyllites (dark grey), test trench T3.

The **Lusatian Fault** displays a complete architecture outlined in the previous Chapter. The central structure of the LF is the *main fault* defined as the dislocation between the footwall and the hangingwall blocks. It consists of the core of the main fault, surrounded by zones of wall-rock brecciation and the footwall and hangingwall damage zones. Much like most major faults worldwide, the LF was activated both before and after the stage of main displacement, and the resulting structures thus now accompany the LF. We therefore find useful to introduce the term **Lusatian Fault Belt** (LF Belt) which includes the LF proper with the associated structures. Four segments of the LF Belt, each having its specific architectural style, can be distinguished along the strike (from W to E): the Elbsandsteingebirge, the Lusatian, the Ještěd and the Jizera segments (Fig. 1).

5.2. Lusatian Fault

The **core of the main fault** is represented by its simplest form at all studied sites: a layer of fault rocks several metres thick, discordant to primary structures of both walls (Fig. 4). The thickest documented outcrops of the fault core display a composite structure of subsidiary layers of fault rocks differing in their parental lithologies (Fig. 5). However, no cases of a multiple fault-core development were encountered.

Grain-size analyses of the fault core (e.g., Horáček et al. 1975) suggested the predominance of chaotic breccias (*sensu* Woodcock and Mort 2008). Fault gouges occurred mostly only within thin smears of principal slip zones, rarely transecting bodies of the core and its vicinity (Figs 4–5). The dominance of chaotic breccias is a significant feature of rocks within the fault core – they were affected by the large fault slip to such extent that no indications of parent-rock structures or geometric fit of adjacent clasts are visible. Matrix of the breccias consists, besides comminuted material, of illite of detrital polytype $2M_1$ and newly formed $1M_d$, kaolinite, chlorite and accessory smectite.

The **zone of wall-rock brecciation** is developed along most of the fault, affecting its both walls to a variable degree. It is a zone-shaped volume of brecciated protolith adjacent to the fault core. The intensity of rock comminution and the proportion of matrix among breccia clasts generally decrease away from the fault core. Three

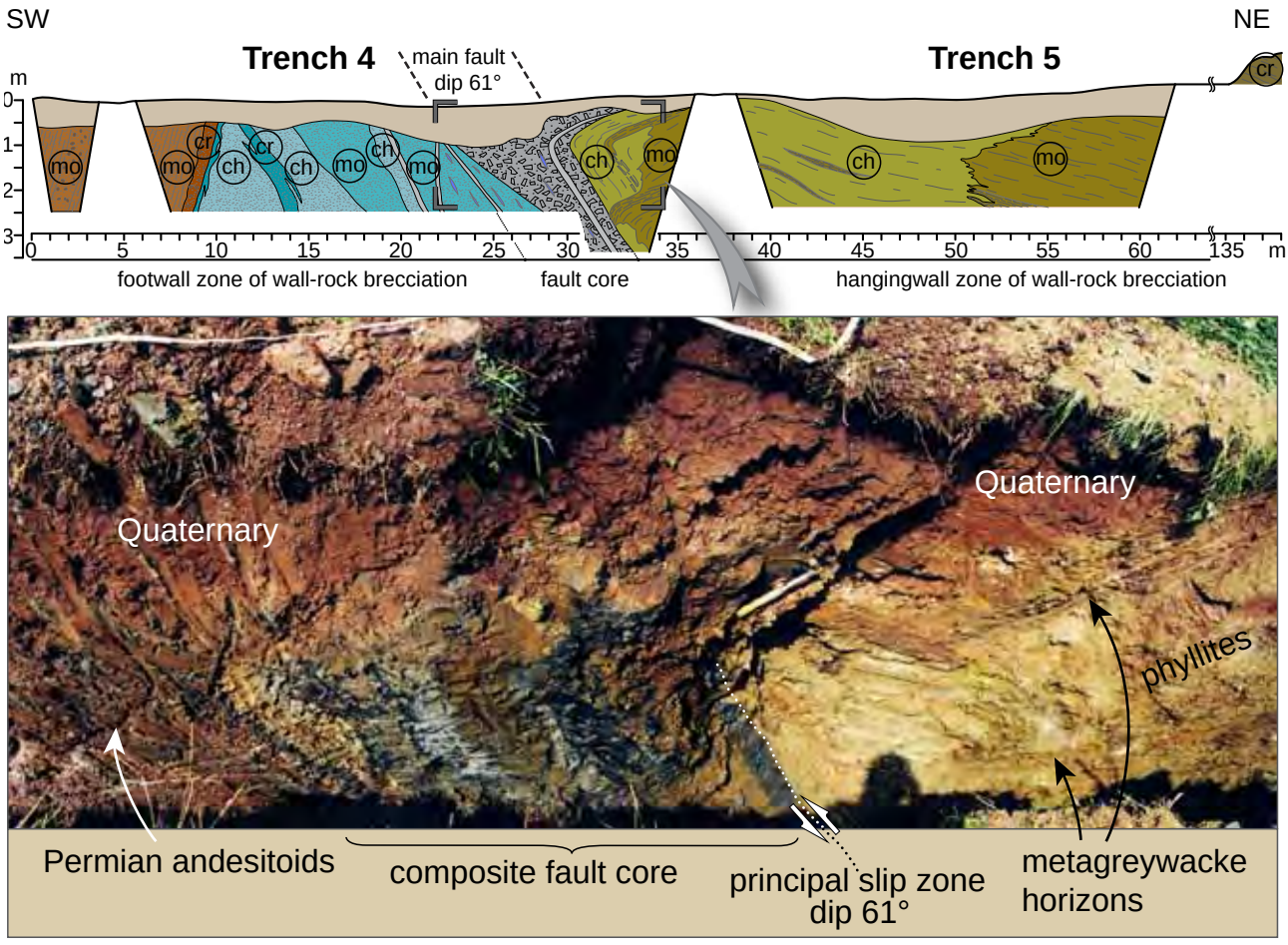

Fig. 5 Main fault and wall-rock brecciation, test trenches and pits T4 and T5 near Site 9. See Fig. 4 for a key. Vertically exaggerated. Photo: A composite structure of the main fault core, with varicoloured bands of chaotic breccias representing different parent rocks. Portions of hangingwall block-derived chaotic breccia can be distinguished from that in the core by the presence of dragged metagreywacke intercalations (right).

sub-zones were distinguished (Figs 4–5), marked by the prevailing type of brecciation (see Woodcock and Mort 2008). The most distant one, lying at the boundary with the protolith, is the crackle breccia in which unaltered rocks are fractured by a dense network of thin cracks. The proportion of matrix among the lithons increases towards the fault core, constituting the mosaic breccia sub-zone. Immediately adjacent to the fault core is the chaotic breccia sub-zone with a substantial proportion of matrix and common effects of clast turbation. A significant feature of the zone of wall-rock brecciation is the presence of clear signs of *in situ* fragmentation in all rocks. Even in the highest intensity brecciation, *in situ* fragmentation is documented by, e.g., crushed lenses of secretion quartz in phyllites which retain their connectivity or by preserved shapes of andesitoid bodies in the Permian volcano-sedimentary complex. The zone of wall-rock brecciation is an architectural element transitional between the fault core and damage zone but closer to the latter in its character (Caine et al. 2010; Faulkner et al. 2010).

The **damage zone** of the LF is developed in the footwall and hangingwall blocks. In the hangingwall block, however, the Alpine structures partly overprinted the Variscan ones. Unfortunately, any study on the discrimination between the Alpine and Variscan deformation patterns in the LF hangingwall block is missing. We therefore abstain from describing the complete architecture of the hangingwall damage zone and concentrate only on the sites revealed by our trenching survey.

The definition of the footwall damage zone of the LF is based on a comparison with distant parts of the footwall block not affected by the LF. It is understood as the rock volume near the main fault where the frequency of fracturing suddenly increases (one fracture per a few metres) and where some of the brittle structures typical of the damage zone appear (see Braathen et al. 2009). The latter include deformation bands, slickensides, different types of minor subsidiary faults and fractures, disjunctive cleavage and lenses.

Deformation bands represent the oldest and areally most widespread type of brittle structures within the

damage zone of the LF. Their thickness varies from less than 1 mm to several centimetres. Most of the bands cut other bands with a visible displacement of a few centimetres, exceptionally up to 20 cm. All arrays of deformation bands are, however, dominated by conjugate pairs of planes which correspond to the maximum shear, as indicated by the sense of displacement. Angle bisectors of the two preferentially activated planes are always parallel to the bedding which is variably rotated in the different parts of flanking structures. This implies that the deformation bands formed prior to the tectonic drag. Deformation bands are also developed in sandstones lacking silica cement well beyond the damage zone (Mertlík and Adamovič 2005).

Another type of structures of the damage zone are arrays of **slickensides**, accompanied by numerous non-striated fractures. Slickensides in sandstones concentrate within the distance of *c.* 300 m from the main fault but slickensides in andesitoids or mudstones occur at considerably longer distances, which illustrates the rheological control on the origin of all types of structures (Shipton et al. 2006). The slickensides are mostly superimposed on the deformation bands. As evidenced by the presence of multiple generations of striae, slickensides show clear signs of multi-generation activation by different paleostress fields. Their parameters and succession allow the reconstruction of the multi-stage kinematic history of the LF (Coubal 1989; Adamovič and Coubal 1999). Non-striated fractures locally merge to form subordinate faults with small magnitudes of throw.

Disjunctive cleavage is a less common type of structure within the damage zone. It has the character of dense jointing with no prominent indicators of shear movement. Cleavage in the Cenomanian sandstones is restricted only to the damage zone adjacent to the main fault, while that in the softer Lower Turonian mudstones extends to a distance of 800–900 m from the fault.

5.3. Lusatian Fault Belt

Some of the structures reaching beyond the basic architectural scheme of the main fault were clearly coeval with the main thrusting. These include: (a) the silicification zone developed in the early stages of thrusting, (b) footwall and hangingwall drag zones and subsidiary faults limiting/entering the drag zones, and (c) bedding-plane slip faults. A widespread group of structures of the LF Belt are accompanying faults and mineralization zones superimposed on the architecture of the main thrusting at younger stages of kinematic history of the fault (e.g., ferruginization zone). Besides, the LF Belt also includes structures clearly pre-dating the main thrusting, such as folds of Late Cretaceous age (Prouza et al. 2013) and a variety of accompanying faults.

5.3.1. Silicification zone

Massive silicification is one of the processes clearly associated with the LF, extending up to *c.* 50–200 m from the main fault. Particularly the syntaxial quartz overgrowths of detrital grains in the footwall-block quartzose sandstones of Cretaceous age passing to quartzites are one of the markers of fault proximity, although silicification products also occur in the hangingwall-block granites. The intensity of silicification is the highest in the immediate proximity (several metres) of the main fault, and gradually decreases away from the main fault even in the same lithology. The thickness of the silicification zone in the footwall-block sandstones usually exceeds that of the zone where deformation bands occur. The mutual spatial relationship between the frequency of deformation bands and the intensity of silicification suggests their simultaneous origin. In general, the intensity of silicification and the thickness of the silicification zone clearly increase eastwards, i.e., from the Elbsandsteingebirge to the Jizera segments of the LF (Tab. 1).

5.3.2. Drag zone in the footwall block

The effects of drag folding observed in the immediate footwall of the LF are a widely distributed phenomenon, producing a variety of specific structures. The two groups of drag structures related to the main fault include dismembered blocks and flanking structures.

Dismembered blocks are tectonic slices composed of deeper lying members of the Upper Cretaceous sedimentary succession, Jurassic or Permian rocks, dragged to a position between the main fault and the footwall block. They are fully separated from their original sites of deposition. Dismembered blocks of Permian and Jurassic rocks are ubiquitous in the Elbsandsteingebirge and Lusatian segments of the LF (e.g., Fediuk et al. 1958) but rare in the Ještěd segment (Krutský 1971) (Fig. 1). Parallelism between the orientation of bedding planes in the dismembered blocks and the orientation of the main fault plane at sites 3 and 5, as well as the conditions revealed by exploratory works at Site 1 (Chrt 1956), imply that most dismembered blocks represent plate-like fragments <100 m thick sub-parallel to the main fault plane.

Footwall blocks in fault proximity are generally formed by Upper Cretaceous psammites or by Permian volcano-sedimentary successions of the Mnichovo Hradiště Basin. With the exception of Permian massive effusives, these were lithologies appropriate for the formation of **flanking structures**. These flanking structures can be found in all segments along the strike of the LF. In spite of the different forms, they share one common feature: asymmetrical increase in the dip of bedding planes towards the main fault plane. This suggests their

Tab. 1 Data on the orientation of the Lusatian Fault plane at the different sites studied

Studied site					Fault plane orientation *(in degrees; dip direction/dip angle)*			
Fault segment	No.	Name	GPS coordinates	Area	Fault trace	Direct measurement	Data type*	**Average**
Lusatian	1	Doubice	50.8944°N 14.4806°E	B	52/16	48/20; 50/15; 52/15	PSZ	**52/16**
	2	Horní Podluží	50.8750°N 14.5339°E	C	43/16	40/14; 43/20; 48/14	FHw	**43/16**
	3	Horní Jiřetín	50.8650°N 14.5794°E		20/16			**20/16**
Ještěd	4	Horní Sedlo	50.8189°N 14.8372°E	A	39/27	35/29; 38/27; 40/25	SBFw	**39/27**
	5	Křižany	50.7417°N 14.9442°E	A B T9		40/30 36/30 38/28	PSZ PSZ PSZ	**38/29**
	6	Jiříčkov	50.6981°N 15.0186°E	T8 BK 506b		19/22; 25/25; 14/21 20/30	PSZ PSZ	**19/22**
Jizera	7	Hodkovice	50.6756°N 15.1017°E	A T1 T3	35/40	36/41 38/39	PSZ PSZ	**35/40**
	8	Frýdštejn	50.6611°N 15.1444°E		31/48			**31/48**
	9	Suché skály Cliffs	50.6361°N 15.2106°E	T4		43/61; 45/67; 46/55	PSZ	**43/61**

* Types of data: PSZ – principal slip zones within the core, FHw – uniform faulting of the hangingwall block close to the core, SBFw – large shear bands cutting the footwall block close to the core.

origin by the drag effect of the hangingwall block rather than a relict of a pre-existing fold structure or as due to a flexural character of the fault. Four different forms of flanking structures can be distinguished being characteristic of the individual fault segments (Fig. 6).

Type A is typically found in the Lusatian segment of the LF. Here, the stratification of Upper Cretaceous sediments in the foreland of the main fault shows almost no signs of drag. Only in the close proximity of the main fault, effects of weak reverse drag are observed with strata dipping gently beneath the main fault plane (Fig. 6a). Closer to the fault plane, the dip angles do not exceed 4–8° to the N. The contact with the main fault plane is often marked by the presence of the above-described dragged dismembered blocks.

Type-B flanking is characteristically developed in the Ještěd segment of the LF (Fig. 6b). The footwall block is affected by normal drag to a distance of several hundred metres from the main fault, with dip of *c.* 20–25°. Near the main fault plane, however, the drag turns into a reverse one, forming a low-amplitude anticline. Strata in Cretaceous sediments dip beneath the main fault plane; northerly dips were observed in the Křižany mine at a distance of at least several hundred metres to the north from the exposed main fault plane (Reichmann 1979). Type-B flanking structures are also occasionally associated with dragged dismembered blocks.

Flanking structures of type C are represented by a pure normal drag of strata (Fig. 6c). They are typical of marginal parts of the Jizera segment. Elsewhere, this type was documented only at Site 4 in the Ještěd segment. Compared to the preceding type, type-C flanking structures are broader and their southern margin (onset of a fold) is combined with the presence of a subsidiary fault. The dip angles of strata within the flanking structure increase rapidly to *c.* 45° already in the proximity of the subsidiary fault and further rise towards the main fault. Unlike in types A and B, faults with the same sense of movement as the drag of the fold appear in type-C flanking structures; they transect the fold at more or less regular intervals, being associated with a sudden increase in the strata dip (see Site 4). No prominent drag of dismembered blocks was observed in this type of flanking.

Flanking structures of type D show a normal drag with steeply rotated strata controlled by the movement at the two faults delimiting the flanking structure (Fig. 6d). One of these is the main fault, and the other is the subsidiary fault also involved in type-C drag. The typical site of type-

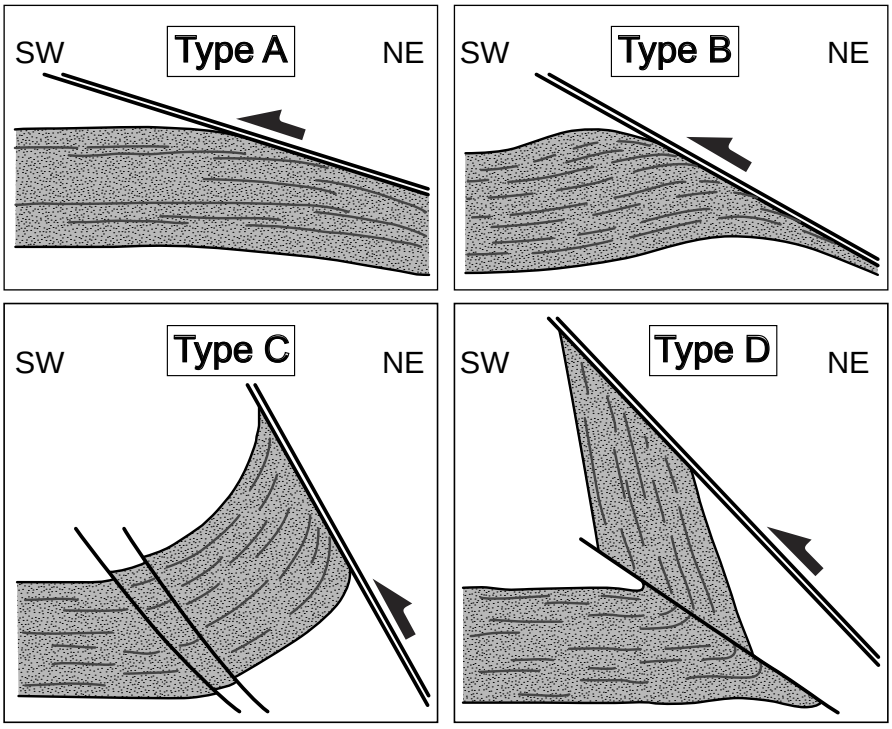

Fig. 6 Cross-sections of the main types of the flanking structures documented in the proximity of the Lusatian Fault. **Type A –** Gentle reverse drag; **Type B –** Normal drag passing to reverse drag in the proximity of the main fault plane; **Type C –** Pure normal drag; **Type D –** Normal drag with steeply rotated strata. Not to scale.

D flanking (Site 8) displays strata overturned to 18° from vertical already at this subsidiary fault. A transition from type-C to type-D flanking structures was probably strongly controlled by an increase in the displacement magnitude along this subsidiary fault. The rotated block is tabular and displays only subtle variations in the dips of strata.

Type-D drag occurs in the central part of the Jizera segment, being manifested by a morphologically prominent, almost continuous belt of Cenomanian sandstones rotated to an upright position. The subsidiary fault limiting the flanking structures of types C and D in this segment is the Frýdštejn Fault – a N-dipping thrust fault with the maximum displacement of *c.* 550 m. It transects the whole Jizera segment, separating steeply rotated to overturned blocks in the N from subhorizontal sediments in the S. Thrust faults offsetting the flanking structures in the proximity of the main fault are herein designated as Frýdštejn-type faults.

5.3.3. Bedding-plane slip faults

Slickensides with striae were also documented on bedding planes of flat-lying sandstones of the footwall block, well outside the damage zone of the LF. They are developed on silicified planes usually following intercalations with elevated clay content or different grain size, separating intervals of homogeneous sandstone several tens of metres thick. These bedding-plane slips are most common in the Elbsandsteingebirge and Lusatian segments of the fault. They were reported by Seifert (1932) and Wagenbreth (1966) from the Elbsandsteingebirge, from a zone 4–6 km broad in the foreland of the LF. Another form of bedding-plane slip in Upper Cretaceous sandstones was reported by Doležel (1976) from the Křižany Mine in the foreland of the Ještěd segment of the LF: a detachment plane along which the overlying Turonian sedimentary package was horizontally transported to the S. In both reported cases, the bedding-plane slips were driven by a NNE–SSW compression, identified as the stress acting during the main thrusting (Coubal 1989; Adamovič and Coubal 1999). Unlike in the above-mentioned segments, bedding-plane slip faults are found only exceptionally in the foreland of the Jizera segment of the LF, e.g., in a wider vicinity of Site 9 (Mertlík and Adamovič 2005; Adamovič and Coubal 2012).

5.3.4. Accompanying faults

A steeply dipping accompanying reverse fault parallel to the main thrust fault of the LF has been reported from several sites on S slopes of Ještěd Hill (Ještěd segment of the LF). It was best described from mine galleries at Site 5. It is a steep reverse fault *c.* 300 m to the N from the main fault, with a fault core markedly thicker (7 m) than the core of the main fault. As suggested by the geological situation, the steep fault is probably an older structure, and is offset by the gently dipping main fault at depth.

Most accompanying faults represent off-sets or modifications of the main fault during subsequent tectonic phases. In all segments of the LF, normal faults postdated

Tab. 2. Thicknesses of architectural elements of the Lusatian Fault Belt

Studied sites			Thicknesses of architectural elements *(in metres)*														
			FOOTWALL BLOCK									MAIN FAULT		HANGINGWALL BLOCK		
			Drag zone		Damage zone				Wall-rock brecciation			Core		Wall-rock brecciation		
Fault segment	Site No.	Area	Type		Disjunctive cleavage	Minor subsidiary faults	Slickensides	Deformation bands	Crackle breccia	Mosaic breccia	Chaotic breccia	Average orientation	Fault breccias and gouges	Chaotic breccia	Mosaic breccia	Crackle breccia
Lusatian	1	A	A	n.d.	n.d.	>29	n.d.		sp	0	0	52/16	2.0	0	sp	>16.5
		B	A	n.d.	n.d.	n.d.	n.d.	<25	<2	0	0		5.3	0	sp	25
	2		A	<130	n.d.	<40	7.8		0	0	0	43/16	2.0	0.3	sp	30
	3		A	<140	n.d.	50–140*	50–140*		sp	0	0	20/16	n.d.	n.d.	n.d.	n.d.
Ještěd	4		C	420	n.d.	340–420*	>230		n.d.	n.d.	n.d.	39/27	n.d.	n.d.	n.d.	n.d.
	5	A	B	470	n.d.	520	340–400*		>5	0	0	38/29	0.6	0–6	<20	n.d.
		B	B	n.d.	n.d.	n.d.	n.d.		n.d.	n.d.	n.d.		3.8	8.0	17	>30
		T9	B	n.d.	n.d.	n.d.	n.d.		18	0	0		>1.5	>5	n.d.	n.d.
	6		B	350	n.d.	250–350*	120–200*		9–15*	0	0	19/22	1.3	2.5	>9	n.d.
Jizera	7	A	C	880	n.d.	800	700	760	n.d.	n.d.	n.d.	35/40	n.d.	n.d.	n.d.	n.d.
		T1	C	n.d.	n.d.	n.d.	n.d.		>7	1–6	0		6.0	2	27	>44
		T3	C	n.d.	n.d.	n.d.	n.d.		>13	12	0		5.6	3.6	8	>13
	8		D	730	490	780	740	580	n.d.	n.d.	n.d.	31/48	n.d.	n.d.	n.d.	n.d.
	9		C	920	850	700	450	500	n.d.	>23.5	16	43/61	5.5	18.5	30–100*	>130

Thickness is given for the core but distances of the outer limit from the core are given for other elements. 0 – element not developed, sp – element sporadically developed, * – value not known exactly but lying within the given interval, n.d. – not determined.

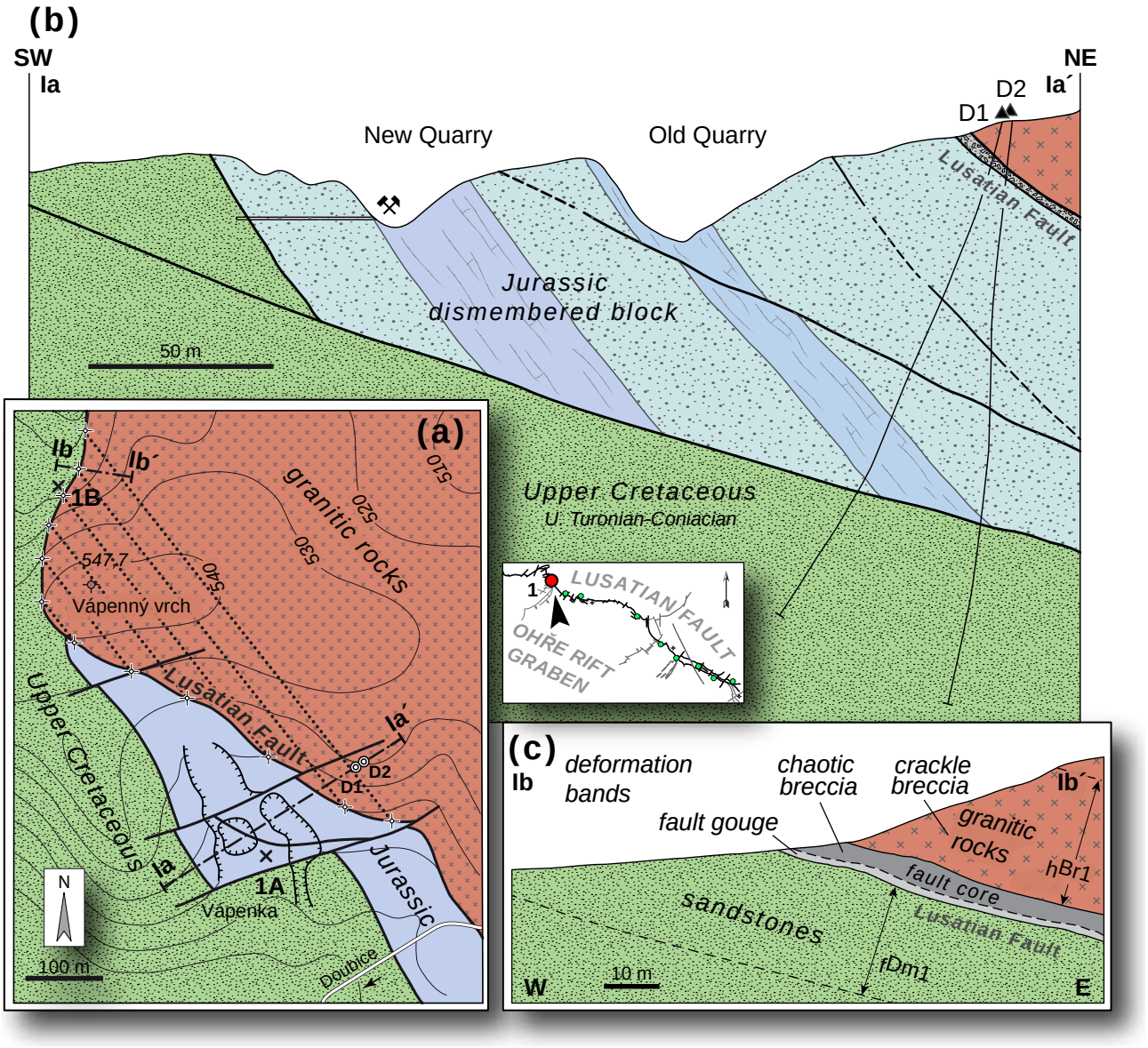

Fig. 7 Lusatian Fault at Site 1 (Doubice). **a –** Geological map showing a dismembered block of Jurassic rocks close to the main fault, dragged from the depth by the movement of the hangingwall block; positions of boreholes D1 and D2 and courses of cross-sections are marked; **b –** A cross-section of the dismembered block parallel to the transport direction at the main fault (after Chrt 1956); (c) a cross-section of the main fault core oblique to the transport direction at the main fault. Horizontal and vertical scales are equal.
Key to the indexes of architectural elements in cross-sections: f – footwall, h – hangingwall; Br – zone of wall-rock brecciation composed of chaotic breccia (Br1), mosaic breccia (Br2) or crackle breccia (Br3); Dm – damage zone composed of deformation bands (Dm1), slickensides (Dm2), minor subordinate faults (Dm3) or disjunctive cleavage (Dm4); Dr – drag zone.

the main thrusting strike parallel to the main fault in both the footwall and hangingwall blocks, forming a more or less pronounced horst. A large population of normal faults transverse to the LF (NNE–SSW) were formed as tensional fractures during the main thrusting and activated during the subsequent tensional stress phase (Coubal 1989; Adamovič and Coubal 1999; Prouza et al. 1999). The most significant of them are the faults limiting the Ohře Rift Graben, locally called the Stráž Fault in the SE and the Doubice Fault Field in the NW (Fig. 1).

5.3.5. Fault-related ferruginization zone

Trenching at the studied sites revealed that most of the fractures in the damage zone are filled with iron oxy–hydroxides (goethite or hematite). In the footwall-block sandstones ferruginization is mostly limited to fillings of transverse faults and extends to a distance of a few tens of metres from the fault core. Ferruginization in the hangingwall-block phyllites is more intense, reaching to *c.* 100 m from the fault core (Fig. 3).

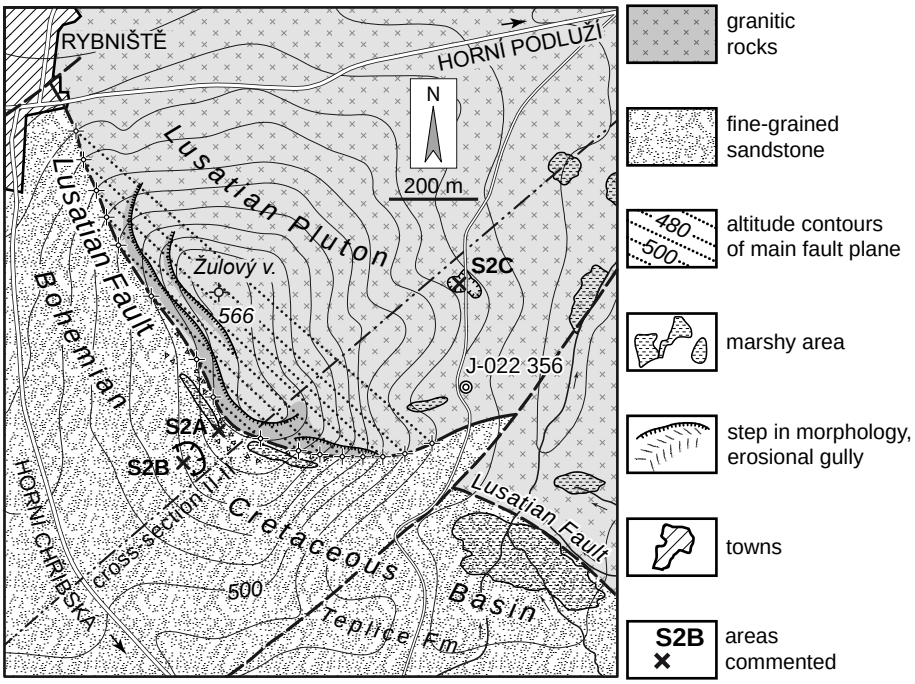

Fig. 8 A geological map of the Lusatian Fault Belt at Site 2 (Žulový vrch Hill near Horní Podluží) showing the characteristic sigmoidal course of the fault trace. For cross-section see Fig. 9.

6. Variations in the architecture of the LF Belt

Characteristic tectonic features of the LF Belt were documented at representative cross sections evenly distributed along the fault strike (Fig. 1). The studied sites are listed below in the order from NW to SE to illustrate the along-strike variations in the LF Belt. Site descriptions also document the methods of data acquisition and the quality of quantitative data used for further considerations. Positions of the sites and their pertinence to fault segments are given in Tab. 1. Quantitative features of the defined architectural elements are summarized in Tabs 1 and 2.

6.1. Factual database

Site 1, Vápenný vrch Hill near Doubice. The LF generally has the character of a simple thrust of the Lusatian granodiorite over Coniacian sandstones. Its architectural elements were studied in two areas within this site (Fig. 7a). In the first of them (S1A), architecture of the fault belt was exposed by quarries and galleries, and verified by additional exploratory works (Chrt 1956). Dismembered blocks of Jurassic and Permian rocks were dragged by the hangingwall-block movement in the immediate footwall of the main fault (Fig. 7b). Jurassic rocks are exposed in a tabular block (Brzák et al. 2007) and deformed by shear fractures of highly variable orientations and by disjunctive cleavage. As revealed by boreholes and a trench in the quarry (Chrt 1956), the layers of fault breccias and gouges of the main fault in the hangingwall of the block, much like tectonic zones at its base, dip at low angles and are very narrow. Cretaceous sandstones exposed by a gallery at the contact with the block are only weakly faulted and local drag of strata is about 14° (Brzák et al. 2007). The second area (S1B) is a continuous transverse profile in a gorge called Jelení rokle (Fig. 7a). The fault core is represented by a layer of chaotic breccia several metres thick, produced by cataclasis of granitic rocks (Fig. 7c). Outside the core, crackle breccia developed in the hangingwall granites gradually passes to protolith over a distance of less than 30 m. Footwall sandstones were deformed by a system of deformation bands in a zone of similar thickness. Outcrops beyond this zone show no faulting. The dip angle of the fault plane is based on the course of the fault trace on the surface (Fig. 7a) and on direct measurements from principal slip surfaces identified in the fault core.

Site 2, Žulový vrch Hill near Horní Podluží. The main fault, separating blocks of similar lithologies as at Site 1, transects the hill in a fault trace indicating its gentle dip to the NE (Fig. 8). Uranium exploration borehole J-022 356 was drilled through 53 m of granodiorite into an almost complete succession of Upper Cretaceous sediments (Fig. 9). The main fault core in the borehole is a thin layer of fault gouge. In the footwall sandstone, this layer is followed by a zone of silicification *c.* 1.5 m thick. The footwall damage zone, represented by slickensides with striae and other signs of intense shear, has been documented in the borehole only to a distance of *c.* 8 m from the fault plane. It can be easily traced in outcrop (Fig. 9) by the characteristic shear structures and the accompanying silicification (S2A). Sandstones beyond the lower boundary of the damage zone, e.g. in quarry S2B,

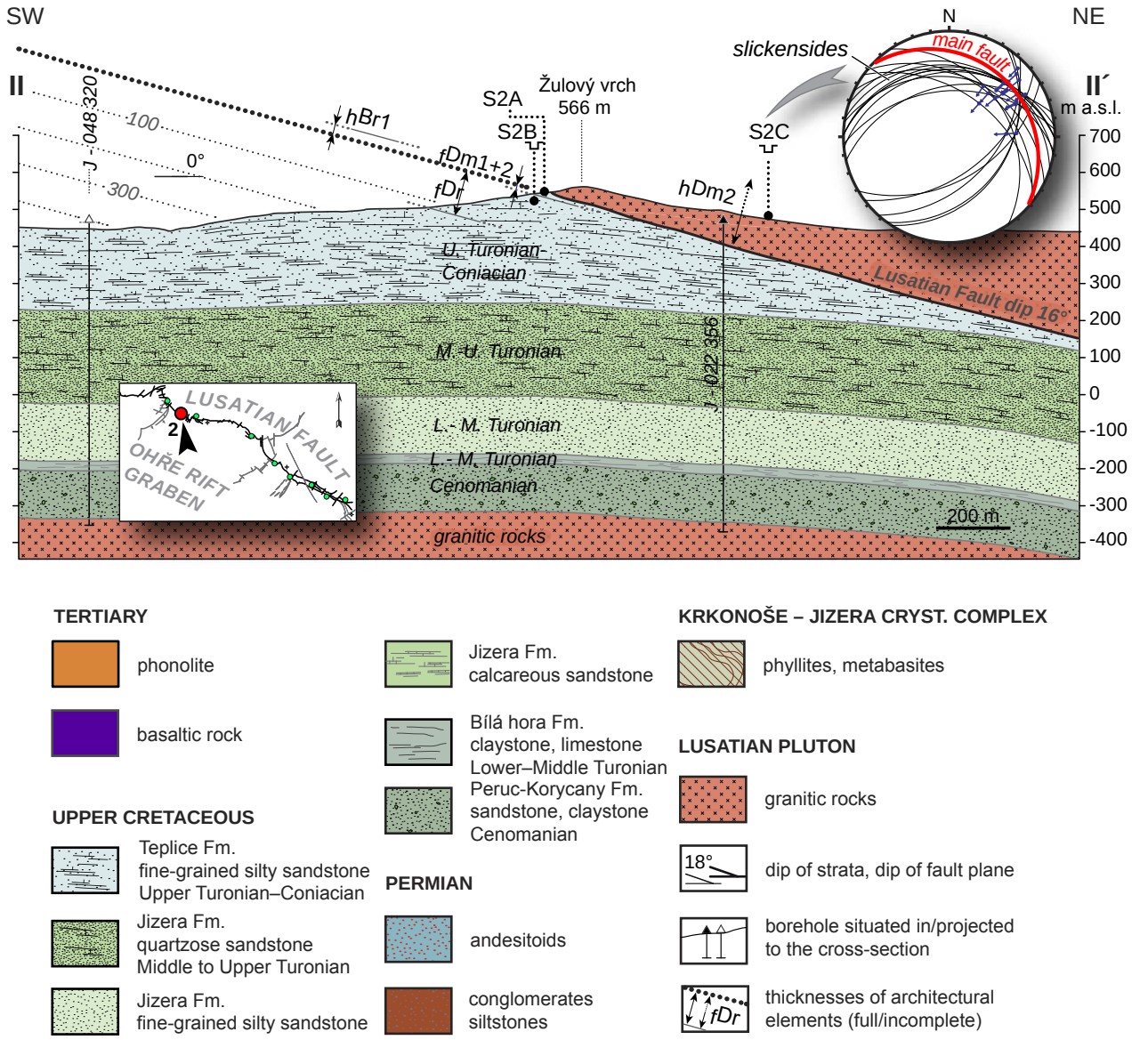

Fig. 9 A cross-section of the Lusatian Fault at Site 2. Dip angle of strata is shown, measured thicknesses of architectural elements are indicated by arrows. Horizontal and vertical scales are equal. For a key to the architectural elements see Fig. 7.

are deformed by regional joints only. Slickensides of the hangingwall damage zone mostly parallel the main fault plane and reach much farther to the hangingwall block, as was observed in quarry S2C.

Site 3, Horní Jiřetín and Jedlová Hill. Old mine workings in the hangingwall block of the LF in the Milířka Valley SW of Dolní Podluží (Fig. 10) were documented by Brzák et al. (2007) who reported a broad damage zone of the main fault with tectonic stacking of blocks of greywacke and granodiorite. The blocks are bounded by faults parallel to the LF and dipping at 25–60°. A low dip angle of the main fault of the LF at this site was inferred from an arched fault trace. A narrow dismembered block of Middle Turonian sandstones was dragged along the main fault and thrust over Coniacian sandstones (Fig. 11). Its base is healed by a Late Eocene phonolite body, which suggests thrusting during the oldest identified tectonic phases of the latest Cretaceous to Paleogene age (Adamovič and Coubal 1999). Sandstones of the dismembered block were deformed by slickensides and minor subsidiary faults (S3A); the adjacent Coniacian sandstones of the footwall block show no visible deformation (S3B). This documents the low thickness of the damage zone.

Site 4, Horní Sedlo near Hrádek nad Nisou. Dip angle of the main fault was determined from a detailed field survey and documentation of test pits; it is also manifested by the dip angle of the dominant shear zones

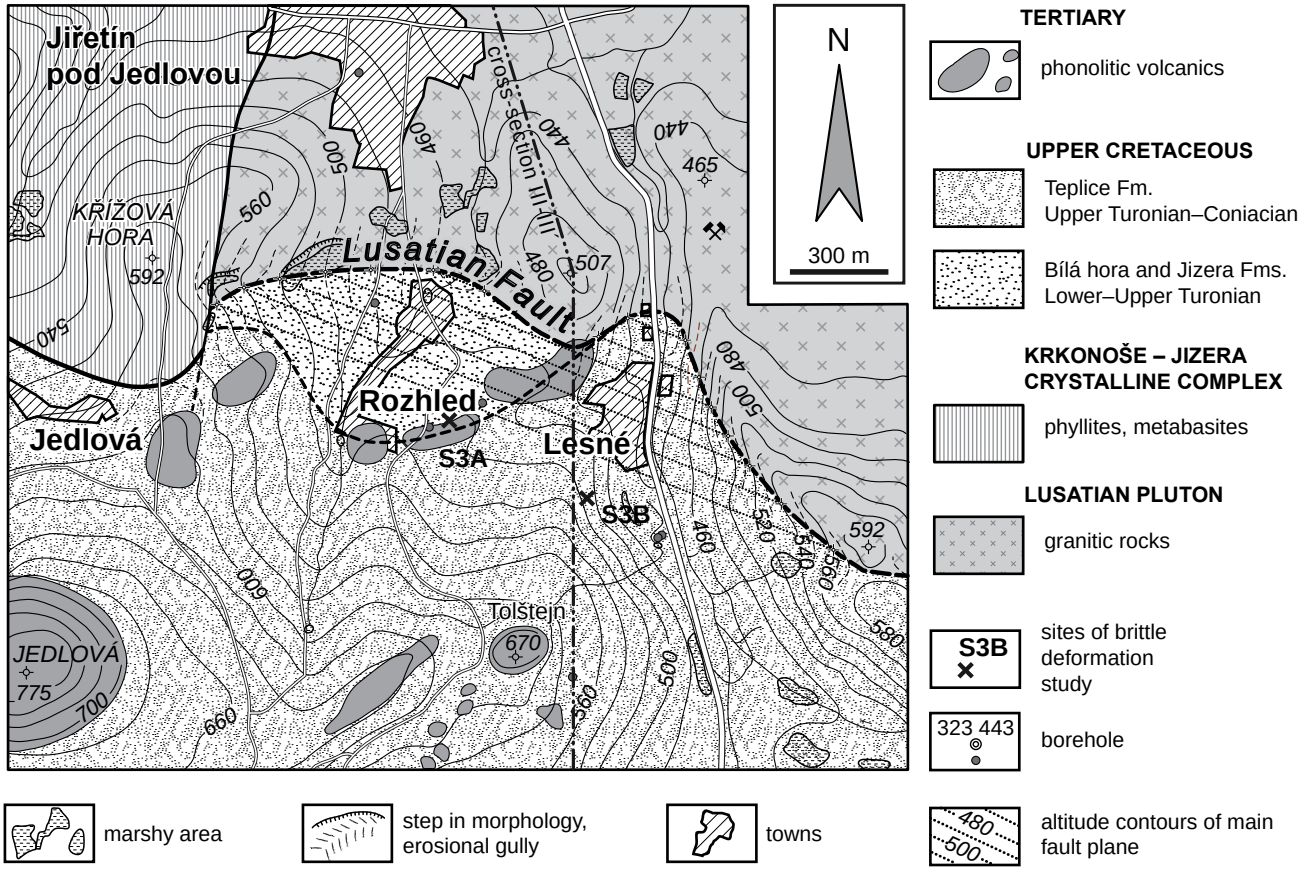

Fig. 10 A geological map of the Lusatian Fault Belt at Site 3 (Horní Jiřetín and Jedlová Hill). For cross-section see Fig. 11.

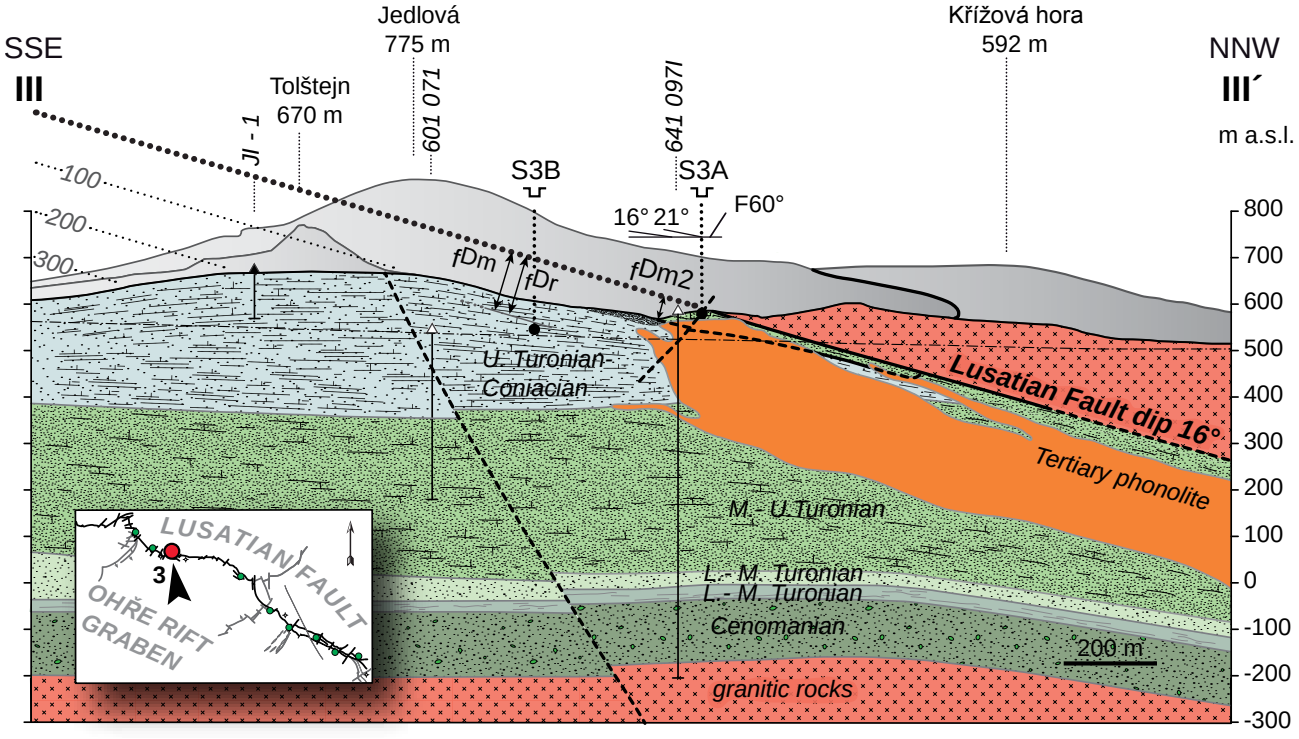

Fig. 11 A cross-section of the Lusatian Fault at Site 3. Dip angles of strata and faults (F) are shown, measured thicknesses of architectural elements are indicated by arrows. Horizontal and vertical scales are equal. For a key to the architectural elements see Fig. 7, to lithologies see Fig. 9.

Fig. 12 Damage zone at Site 4: a shear band cutting Cretaceous quartz-cemented sandstone in the footwall block.

cutting the adjacent Cretaceous sandstones (Fig. 12). Rather rarely for the Ještěd segment, a continuous zone of normal drag is developed along the LF at this site. A stepwise increase in the dip of the footwall-block Turonian sandstone strata is observed within the flanking structure at a set of Frýdštejn-type faults (Fig. 13). The sandstones show sets of deformation bands (S4A), whose density decreases away from the main fault (S4B), and less common slickensides of the damage zone.

Site 5, Křižany. Architecture of the LF at Křižany is relatively well known based on the exploratory works for barite–fluorite (area S5A, Reichmann 1979), as well as exploration and mining works for uranium (area S5B, Bělohradský and Petrin 1977) and limestone (Sedlář and Krutský 1963). The dip of the main fault was verified by a set of test pits T9 (Prouza et al. 1999). All technical works found the core of the main fault to dip NNE at low to moderate angles (Fig. 14a). In the TP-1P gallery of the uranium mine the main fault core has a character of a chaotic breccia zone (Fig. 15). Matrix of the breccia was reported to be composed of disintegrated Cretaceous siltstones with dispersed carbonaceous matter, whereas the clasts consist of rounded quartz fragments and crushed fluorite–carbonate mineralization (Reichmann 1979). Thickness of the fault core at this site ranges from a few tens of centimetres (Reichmann 1979; Prouza et al. 1999) to 4 m (Bělohradský and Petrin 1977). Another prominent fault dipping 50–70° NE with a considerably thicker core (7–9 m) was documented in the mine several hundred metres NE of the LF (Rousek and Týlová 1956). This steep subsidiary fault has been identified at several other sites in the Ještěd Hill area (Bělohradský and Petrin 1977). Apart from the above-described localities, Site 5 displays products of *in situ* brecciation of hangingwall phyllites adjacent to the core. Chaotic breccia in phyllites of the hangingwall block was only exceptionally documented in zones up to 6–8 m thick (Rousek and Týlová 1956; Bělohradský and Petrin 1977). In most outcrops, the wall rock brecciation is manifested only by mosaic breccia and especially crackle breccia. Flanking structure of Type B dominates the footwall drag zone

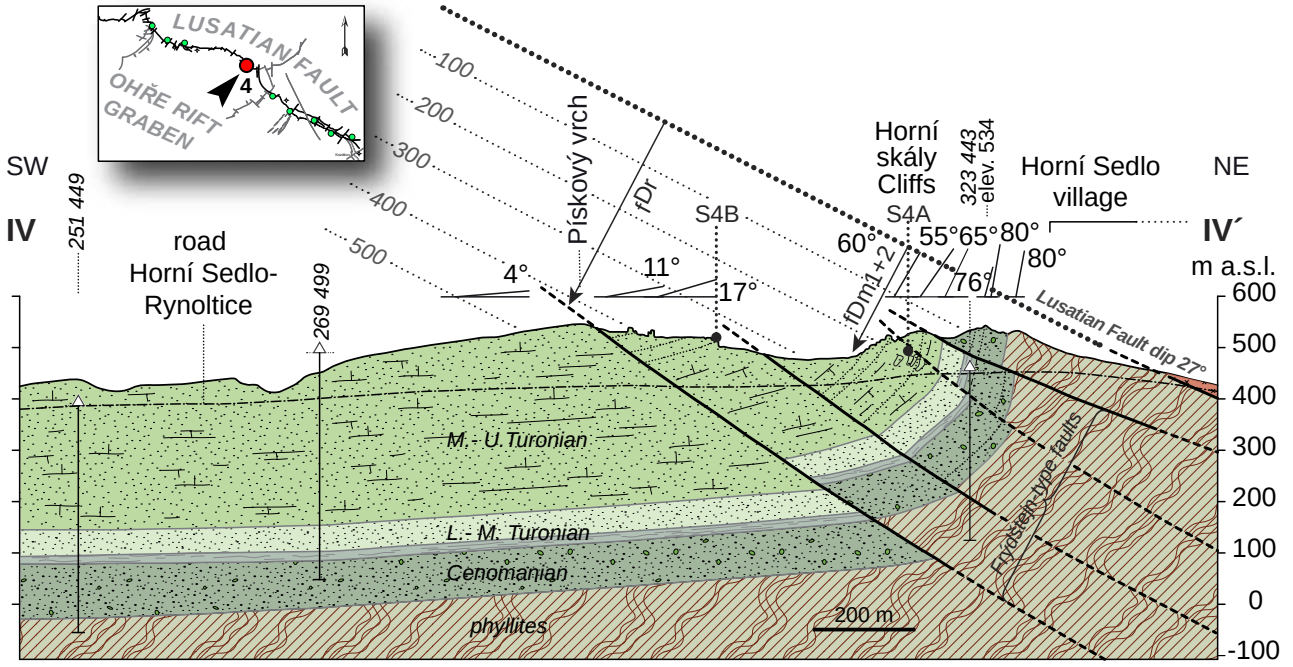

Fig. 13 A cross-section of the Lusatian Fault at Site 4 (Horní Sedlo near Hrádek nad Nisou), showing a typical flanking structure dominated by normal drag. Dip angles of strata are indicated, measured thicknesses of architectural elements are indicated by arrows. Horizontal and vertical scales are equal. For a key to the architectural elements see Fig. 7, to lithologies see Fig. 9.

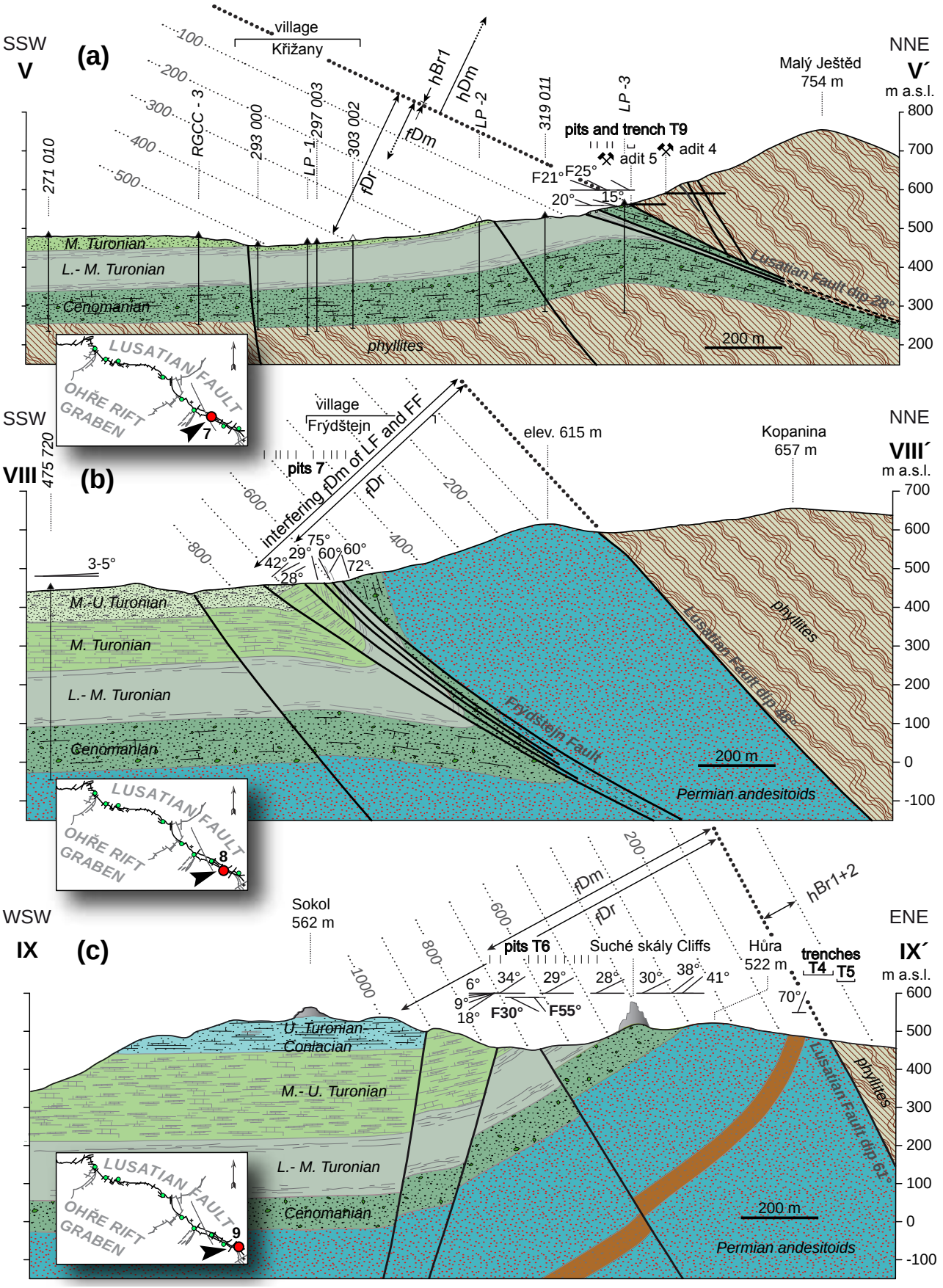
SSW
V
(a)
NNE
V´
village
Křižany
Malý Ještěd
754 m
m a.s.l.
RGCC - 3
271 010
293 000
LP -1
297 003
303 002
hBr1
hDm
LP -2
fDm
fDr
319 011
LP -3
pits and trench T9
adit 4
adit 5
F21°
F25°
20°
15°
M. Turonian
L.- M. Turonian
Cenomanian
phyllites
Lusatian Fault dip 28°
200 m
LUSATIAN FAULT
OHŘE RIFT GRABEN
7
SSW
VIII
(b)
NNE
VIII´
village
Frýdštejn
475 720
pits 7
interfering fDm of LF and FF
fDr
elev. 615 m
Kopanina
657 m
3-5°
75°
29°
60°
60°
42°
72°
28°
M.-U. Turonian
M. Turonian
L.- M. Turonian
Cenomanian
phyllites
Lusatian Fault dip 48°
Frýdštejn Fault
200 m
Permian andesitoids
LUSATIAN FAULT
OHŘE RIFT GRABEN
8
WSW
IX
(c)
ENE
IX´
Sokol
562 m
fDm
fDr
hBr1+2
pits T6
Suché skály Cliffs
Hůra
522 m
trenches
T4
T5
m a.s.l.
6°
34°
29°
28°
30°
38°
41°
9°
18°
F30°
F55°
70°
U. Turonian-Coniacian
M.- U. Turonian
L.- M. Turonian
Cenomanian
Lusatian Fault dip 61°
phyllites
200 m
Permian andesitoids
LUSATIAN FAULT
OHŘE RIFT GRABEN
9

⇦

Fig. 14 Cross-sections of the Ještěd and Jizera segments of the Lusatian Fault. **a –** Site 5 (Křižany), **b –** Site 8 (Frýdštejn), **c –** Site 9 (Suché skály Cliffs near Turnov). Dip angles of strata and faults (F) are indicated, measured thicknesses of architectural elements are indicated by arrows. Horizontal and vertical scales are equal. For a key to the indexes of architectural elements see Fig. 7, for a key to lithologies see Fig. 9.

Fig. 15 A layer of chaotic breccia forming the core of the main fault surrounded by the footwall and hangingwall damage zones exposed in the Křižany mine (Site 5). Photo courtesy of Ferry Fediuk. For a more detailed description of the breccia, see text.

(Fig. 14a). All test pits at this site revealed the presence of reverse drag in beds of Cretaceous sediments immediately beneath the main fault plane (Sedlář and Krutský 1963; Prouza et al. 1999).

Site 6, Jiříčkov. This site is significant for the determination of lateral extent of the architectural elements as it lies immediately W of an important transverse feature – the Devil's Walls dyke swarm (Fig. 1). It displays architecture of the LF Belt (Fig. 16) typical of the Ještěd segment. In test trench T8 (Prouza et al. 1999), the main fault plane was found to dip gently NNE, as has been already documented by previous test trench BK 506b (Bělohradský and Petrin 1977). Much like at most other sites of the Ještěd segment, the low-angle plane of the main fault is associated with dismembered blocks. Blocks of Permian rocks were reported from this site by Sedlář and Krutský (1963) and Krutský (1971). In the hangingwall phyllites, intense brecciation dominated by chaotic breccia was documented in a zone only 2–3 m thick adjacent to the main fault in both above mentioned test trenches. As shown by test trench T8, a continuous flanking structure of Type B with gently dipping strata also contains evidence for reverse drag in the immediate vicinity of the main fault. The footwall damage zone is represented by a zone of crushed sandstone close to the main fault plane, cut by numerous Riedel shears. At a distance of several metres from the fault plane, crushing is replaced by sparse subordinate faults transecting quartz-cemented sandstones.

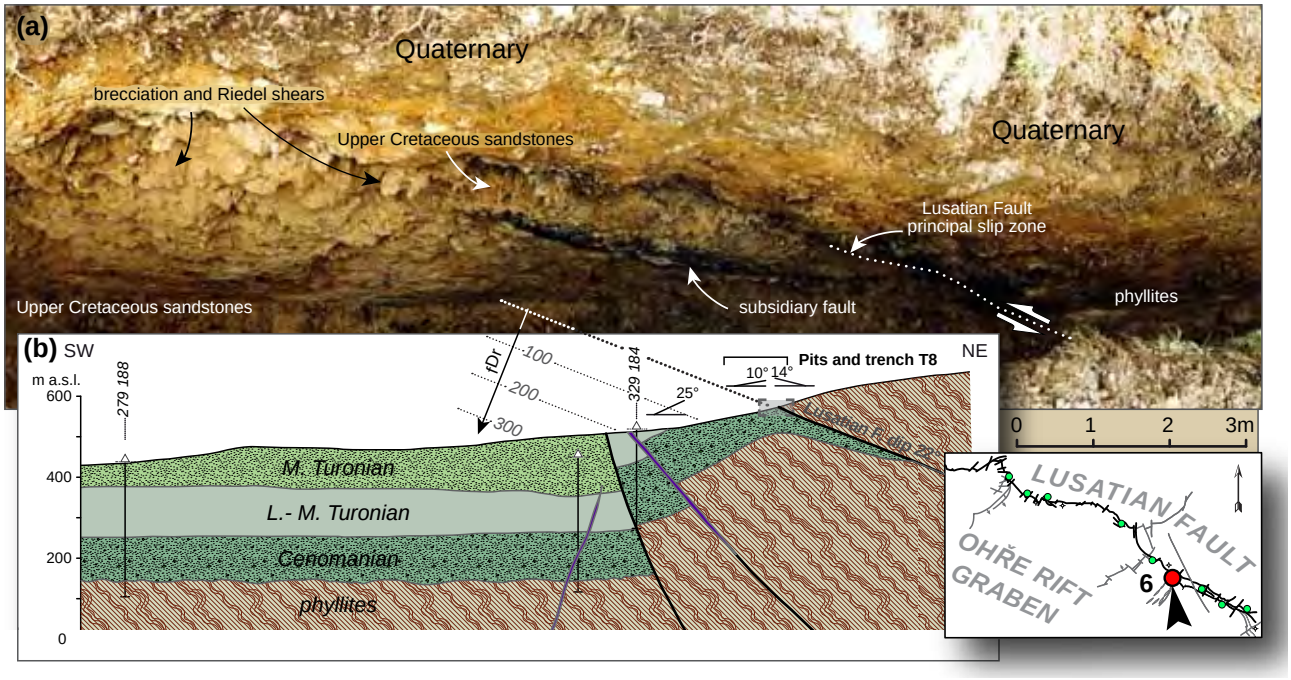

Fig. 16 Lusatian Fault at Site 6 (Jiříčkov). **a** – Gently dipping, narrow core of the main fault, as revealed by test trench T8; **b –** A cross-section indicating the dip angles of strata. Measured thicknesses of architectural elements are indicated by arrows. Horizontal and vertical scales are equal. For a key to the architectural elements see Fig. 7, to lithologies see Fig. 9.

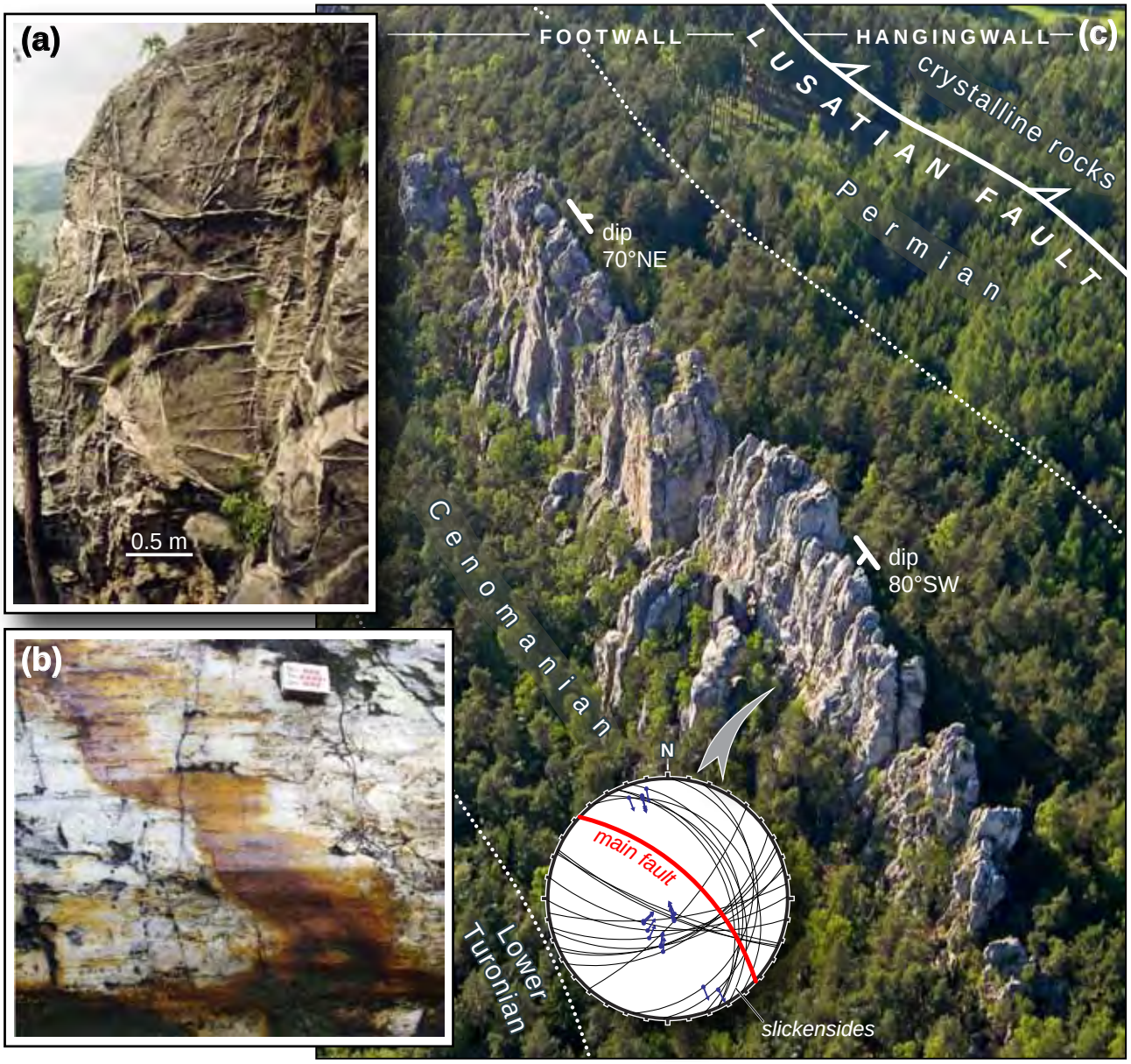

Fig. 17 Architectural elements of the LF exposed at Suché skály Cliffs (Site 9). **a–b** – Typical members of the footwall damage zone cutting the quartz-cemented sandstones of the ridge: deformation bands (a) and slickensides, matchbox for scale (b). **c** – An aerial photograph of prominent steeply dipping bedding planes of Cenomanian sandstones. In the distant part of the photo, bedding planes are overturned at the summit of the cliffs. The course of the LF was determined by trenching.

Site 7, Hodkovice nad Mohelkou. Southeast of Ještěd Hill, the LF Belt was studied in a natural outcrop along the Mohelka River (S7A, Fig. 1). Between the Mohelka River and the Devil's Walls dyke swarm, test trenches T1–T3 were excavated by Prouza et al. (1999), revealing an architectural style of the LF Belt different from that at sites 1–6. The dip of the main fault plane is evident from the course of the fault trace on the W slope of the valley and from the trenches. The core of the relatively steep main fault has a complex structure, including a layer of fault rocks of the main fault core and extensive, irregular bodies of breccias (Fig. 4). Cataclasis of rocks of both blocks is prominent, reaching far from the fault core, gradually passing from chaotic breccia near the core to crackle breccia in more distant parts. Permian volcano-sedimentary complex in the broad footwall drag zone displays relatively steep dips of strata. Their further northward steepening is discontinuous, affected by faults of the Frýdštejn type subparallel to the LF Belt. The steepest dip angles of *c.* 60° are present in the proximity of the main fault. The drag zone was modified by the Frýdštejn Fault, which roughly coincides with its southern limit. The damage zone, also approximately limited by the Frýdštejn Fault in the south, is represented

by simple arrays of sparse deformation bands cutting the sandstones and by minor subsidiary faults.

Site 8, Frýdštejn. The trace of the main fault plane on the surface at Frýdštejn (Fig. 14b) indicates its relatively steep dip. A relict of the hangingwall-block phyllites overlying an exhumed fault plane is exposed here. The footwall block in the immediate southern foreland of the main fault is represented by Permian andesitoids (Fig. 14b). Intense faulting of the damage zone including numerous subsidiary faults with cores tens of centimetres thick, a network of slickensides, and brecciation were observed across the whole width (*c.* 580 m) of the area. The drag zone is built by Cenomanian sandstones overlying the andesitoids. Their strata are rotated to near-vertical dip or even overturned. The southern limit of the drag zone of the main fault is – much like at Site 7 – close to the Frýdštejn Fault, along which steeply dipping formations were thrust over subhorizontal Cretaceous sediments. The architecture of the Frýdštejn Fault was studied by a series of test pits T7 (Prouza et al. 1999): it has the character of a *c.* 200 m wide, intensely fractured zone combining the damage zones of both faults.

Site 9, Suché skály Cliffs near Turnov. This site illustrates the architecture of the Jizera segment of the LF Belt (Fig. 14c). The core of the main fault in its full thickness was exposed by trenches T4 and T5 (Fig. 5). The main fault has a character of a layer comprising many individual zones of different composition. Argillized parts of the walls are pervaded by younger veins, lenses and concretions of hydrothermal carbonates, and show signs of intense ferruginization. The dips of the fault core are the steepest of all documented along the whole LF main fault. It is lined with broad zones of wall-rock cataclasis on both sides. The prominent crest of the Suché skály Cliffs (Fig. 17) is formed by footwall-block Cenomanian sandstones subjected to intense silicification. These provide an excellent opportunity to study the drag zone and the damage zone of the main fault. Both of them display effects of intense faulting and continuum deformation extending to many hundreds of metres from the main fault. The damage zone is represented by arrays of deformation bands of a variable density, slickensides of several generations (Fig. 17a–b), disjunctive cleavage, and locally by brecciation of rocks. The drag zone displays rotation of strata within the flanking structure with an abrupt steepening of dip angles towards the main fault, reaching an overturned position of 70° to the NE (Fig. 17c). This trend in dip angles of strata (Fig. 14c) was documented by a series of test pits T6 (Prouza et al. 1999). The outer limit of the drag zone is defined by one of the branches of the Frýdštejn Fault. This fault, which parallels the LF in its footwall block at sites 7 and 8, splits into a number of branches here. These transect the LF and continue further east in the hangingwall block (Fig. 1).

6.2. Variability of architectural elements and tendencies inferred from factual database

Information on the dip angle of the main fault at the studied sites is summarized in Tab. 1. Among the different methods of dip measurement, the highest credibility was given to the determination of fault trace in the field because it was not affected by post-faulting processes (e.g. solifluction).

The table clearly shows that the dip angle of the main fault generally increases from NW to SE. This increase is not continuous: some segments show internally comparable dip angles (e.g., Sites 1–3) while a marked change in the dip angle is observed between Sites 6 and 7, i.e., between the Ještěd and Jizera segments.

Table 2 presents the thicknesses of architectural elements of the LF Belt, as reconstructed from field observations and archival data. Even the minimum thickness estimations are given in case they illustrate the variation in the size of architectural elements. Besides Tab. 2, the thicknesses are graphically presented in cross-sections to the individual sites. As shown in Tab. 2, thicknesses of architectural elements in the hangingwall block are distinctly greater than their counterparts in the footwall block. This applies to the Lusatian and Ještěd segments, while in the Jizera segment the thicknesses are about equal. We concentrated on the architecture of the central and footwall parts of the LF; consequently, only data from zones adjacent to the fault core and exposed by trenching are reported from the hangingwall block.

Wall-rock brecciation in the hangingwall block in the Lusatian segment is dominated by crackle breccia in a zone a few tens of metres thick, with chaotic breccia being observed only exceptionally in negligible thicknesses. In the Ještěd segment, the zone of wall-rock brecciation has a similar thickness as in the Lusatian segment; however, chaotic breccia sub-zone was documented at higher thicknesses of 6–9 m. In the Jizera segment, the observed brecciation intensity is much higher compared to those in the preceding segments. Parts of this zone composed of mosaic and chaotic breccia are commonly up to several tens of metres thick.

The **fault core** in the Lusatian and Ještěd segments is represented by a contrasting layer of fault rocks tens of centimetres to max. 5 m thick, contrasting with the weakly deformed wall rock. In the Jizera segment the thickness of the fault core is clearly higher but mostly ranges within a few metres. A simple layer of fault rocks passes eastward into a more complex internal structure with multiple layers of different fault rocks. The contrast between the core and adjacent portions of the hangingwall and footwall blocks becomes less prominent due to the presence of wall-rock brecciation. A systematic change in the thickness of the core can be, however, hardly seen based on the presented data.

Footwall-block sediments at contact with the core suffered almost no brecciation in the Lusatian segment, while a zone of sandstone brecciation over 10 m thick was documented in the Ještěd segment. In the Jizera segment, its thickness increases to tens of metres, with common presence of chaotic breccia. This increase in thickness is prominent between Sites 6 and 7, even though a change in the lithology of rocks at the fault plane can be also supposed to play a role.

According to Shipton et al. (2006), variations in the thickness of the **damage zone** should be evaluated separately for its individual subzones because their thicknesses are not equal. The thickness of the subzone formed by subsidiary faults in the LF Belt was generally found to be markedly higher than that of the subzone formed by deformation bands and slickensides. In the Lusatian segment, only a narrow damage zone is developed, featuring all characteristic types of structures. In the Jizera segment, the gradual increase in the thickness of the footwall-block damage zone is marked by the subzone of dense deformation bands and slickensides; these can be found over distances of many hundreds of metres from the main fault. In this segment, the thicknesses of the part of the damage zone formed by subsidiary faults and that of the drag zone are about equal and both of them markedly increase towards the E. Disjunctive cleavage, absent in the Lusatian and Ještěd segments, appears in the footwall damage zone of the Jizera segment. In soft rocks at Site 9, it was found to reach the farthest from the main fault of all damage zone members – almost 900 m.

A prominent alongstrike variation can be seen in the **drag zone**. In the Lusatian segment, the presence of a very gentle reverse drag (Type A) is manifested by the regional dip of Cretaceous sediments to the N. The Ještěd segment is dominated by a normal drag zone, which induced a flanking structure with a shallow dip of 15–25°. In the flanking structure adjacent to the fault plane, however, normal drag changes for a reverse one (Type B) and dismembered blocks occur. Drag zone in the Jizera segment is formed solely by normal drag (Type C). No dismembered blocks or reverse drag were found within the flanking structure in fault proximity; instead, strata are locally overturned. The thickness of the drag zone in the Jizera segment reaches the highest encountered values. A local drop in its thickness around Site 8, much like a change in its shape (Type D), resulted from its shortening by thrusting at the Frýdštejn Fault.

In summary, the intensity of deformation and the thickness of most architectural elements in the LF Belt increase to the SE. This holds particularly for the zones of wall-rock brecciation in the footwall and hangingwall blocks, for the individual subzones of the footwall damage zone and for the drag zone. This trend is compatible with the increase in the dip angle of the main fault.

7. Discussion

In general, the character and the thickness of architectural elements of major faults have been documented to vary along the fault strike (Caine et al. 2010). Based on these variations at a local scale, general trends in fault architecture can be traced regionally. Tectonic studies of major faults should be therefore based on a wider range of structures characteristic of their architectural elements (Shipton et al. 2006). Several factors controlling the fault architecture have been suggested, including the lithology of wall rocks (Shipton et al. 2006) and the presence of inhomogeneities such as layering, variable clay content, mineralization or previous fabrics. A special attention has been given to the thicknesses of the fault core and damage zone as a function of the fault displacement magnitude (Shipton et al. 2006; Childs et al. 2009; Faulkner et al. 2010; Torabi and Støren Berg 2011). Another factor controlling the architecture of the fault is the orientation of stress relative to the fault plane and the consequent relation between its shear and normal components, the magnitude of stress, depth of formation or fluid pressure (Faulkner et al. 2010).

7.1. A dynamic model of the origin of the Lusatian Fault Belt architecture

It has been shown that reactivation of a fault with alongstrike dip changes by stress of a homogeneous orientation can be held responsible for variations in the fault belt architecture, e.g., thicknesses of the damage zone and the drag zone. This idea is in a good agreement with our observations from the LF: the inferred stress shows no variation among the separate fault segments with different fault plane dip angles; however, shear and normal stress components do vary in their orientation and magnitude. Particularly the variation in the normal stress component played a decisive role in the origin of the observed fault belt architecture.

Both essential factors of this model, i.e. paleostress parameters and dips of the main fault, were studied. As revealed by paleostress analysis (Coubal 1989; Adamovič and Coubal 1999; Prouza et al. 1999), the thrusting was driven by compression $\boldsymbol{\alpha_1}$ with maximum compressive stress σ_1 plunging SSW at an average angle of 10–20°. Also the geometry of the rotation of strata in the footwall drag zone suggests that the flanking structures were formed within the main thrusting episode, in the earliest stage of the reconstructed succession of deformation events.

During tectonic events, rock massifs display stress states which can be described by stress tensor σ. Each arbitrarily orientated plane of the stressed body is subjected to stress vector **S** determined by the relation

$$\mathbf{S} = \sigma \cdot \mathbf{n},$$

where **n** is the unitary vector normal to the plane. Generally, there are three planes for which the stress **S** is perpendicular to the plane defining three axes of the tensor σ. Stress **S** acting on the main fault plane can be decomposed into a shear component S_s which tends to produce slip along the fault plane, and a normal component S_n which presses the two blocks against each other (Fig. 18). As soon as the shear stress S_s exceeds the friction on the fault plane (which is proportional to the normal component S_n), slip occurs along the fault. This can be expressed by relation:

$$\mathbf{S}_s \text{ (critical)} = \mu_s \mathbf{S}_n,$$

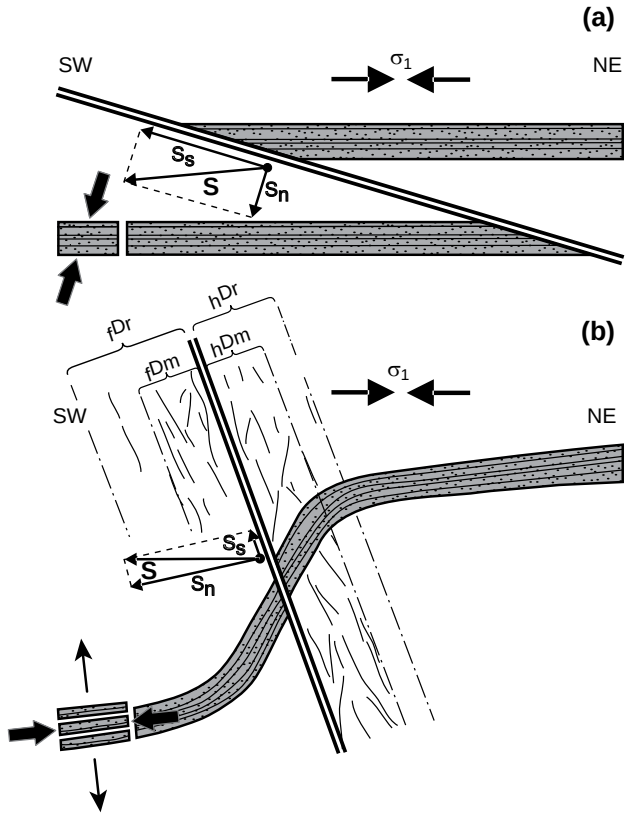

Fig. 18 Variations in stress distribution near the fault plane depending on its dip angle, in cross-sections. See explanation in text. **a** – Shallowly dipping main fault, normal stress component sub-perpendicular to bedding planes of the footwall-block sediments; **b** – Steeply dipping main fault, normal stress component sub-parallel to bedding planes. **S** – stress vector acting on the fault plane, S_s – shear component of this stress vector, S_n – normal component of this stress vector. For a key to the architectural elements see Fig. 7.

where μ_s is the friction coefficient. At real faults, the friction coefficient depends on many factors such as morphological irregularities of the fault plane, presence of clay, fluids and so on. If slip occurs on the main fault, the magnitude of the shear stress on the fault plane becomes partly reduced. On the contrary, the magnitude of the normal stress component remains the same. This means that the stress tensor is changed and one of its main axes becomes nearly perpendicular to the fault plane.

The nature and the thickness of the damage zone are, besides other factors, controlled by the magnitude of stress, which affects the surroundings of the main fault. Pre-existing interfaces near the main fault (minor faults, fractures, sedimentary strata boundaries etc.) are of various orientations. If their orientations are more favourable for shear movement, these interfaces become less resistant to the acting stress tensor then the main fault itself. Then, fractures inside the damage zone become reactivated. As the maximum frequency of pre-existing fractures and minor faults concentrates along the main fault (as a consequence of non-uniform movement at the main fault), repeated movement is the most intense near the main fault.

The magnitude of the stress which can be reached in the damage zone is controlled mainly by two parameters: the stiffness of the main fault and the normal stress affecting the fault zone. If the normal component of stress is small (Fig. 18a) and the stiffness of the fault is low, almost all movements take place on the main fault and the damage zone is very narrow, represented only by irregularities of the main fault. If the normal component of stress is small but the stiffness of the main fault is high (e.g., locked by an asperity), reactivation of fractures of the damage zone parallel to the main fault can occur. This phenomenon can be observed at Site 2 (Fig. 9).

Finally, if the normal component of stress is large compared to the shear component (Fig. 18b), the probability of movements at subordinate faults of other orientations (not parallel to the main fault) is high. In that case, a wide damage zone develops with a high frequency of subordinate active faults of various orientations. The resulting movement at fractures of the damage zone can compensate for the insufficient displacement at the main fault. At the LF, this mechanism affects the steep segments of the main fault – see Site 9 (Fig. 17).

Moreover, variations in stress distribution along unequally orientated segments of a reactivated fault imply variable conditions for the formation of the drag zone. In fault segments with low dip angles of the fault plane (Fig. 18a), a minor portion of shear stress was transmitted from the reactivated main fault to the wall rock due to the relatively small normal stress component. As a result, thrusting of the hangingwall block over Cretaceous sediments in fault segments with low dip angles was not

associated with a significant deformation of strata in the footwall block (Figs 9, 11). With the increasing dip angle (Fig. 18b), the normal stress component increases and higher shear stress becomes transmitted to both the hangingwall and footwall blocks. This resulted in the origin of type-B flanking structures along a moderately dipping fault (Ještěd segment, Fig. 14a) or type-C a flanking structures along steeply dipping fault segments (Jizera segment, Figs 13, 14c). The deformation of these structures was also enhanced by the effect of relatively large normal stress component at steep segments of the fault: a prominent pure-shear deformation in the footwall block (Fig. 14b).

Variations in the thickness of both the damage and the drag zones can also reflect the variable degree of detachment of the underthrust sedimentary packages. In fault segments characterized by low dip angles (Fig. 18a), normal stress component acted sub-perpendicular to the bedding planes of the footwall-block sediments, thereby supporting the integrity of the underthrust sedimentary package. In steep fault segments (Fig. 18b), however, the normal stress component was larger and acted sub-parallel to the bedding planes. The individual members of the sedimentary package became detached from one another by the effect of induced transverse extension. Detachment of the package members in fault vicinity results in the reduction of stiffness of these packages which can be subsequently more easily integrated into both the drag and the damage zones.

7.2 Origin of the complex structure of the Lusatian Fault Belt

The field-mapping in the past decades postulated that the LF coincides with the present northern limit of the Permian to Cretaceous fill of post-Variscan basins. This assumption was validated only in the Elbsandsteingebirge segment of the fault which lacks flanking structures. In other segments, the flanking structures in the footwall block combined with gentle to moderate northerly dips of the main fault may expose steeply dipping basinal sediments transgressively overlying crystalline rocks (see Fig. 13c). At such sites, the main fault lies further N, separating crystalline rocks of the footwall from those of the hangingwall block (Fig. 19b), as proved by the trenching survey.

A detailed analysis and a comparison of the nature of individual architectural elements revealed that differences in stress distribution around unequally orientated segments of the main fault were the principal controlling factor of alongstrike variations in the architecture of the whole fault belt, including the notable contrast between its NW and SE parts (Fig. 20).

In the **Lusatian segment**, gentle northeasterly dips of the main fault were favourable for shear activation under the α_1 compression acting during the main thrusting (Coubal 1989; Adamovič and Coubal 1999; Prouza et al. 1999). This resulted in the formation of a flat thrust fault (Fig. 20a). The main fault is accompanied by only a very narrow damage zone, and the footwall block in the proximity of the main fault shows effects of a low intensity of deformation and a patchily developed quartz cementation in a zone of several metres from the main fault (Tab. 1, Figs 9, 11). Drag structures associated with low-angle thrusting are limited to isolated dismembered blocks of Cretaceous, Jurassic and Permian rocks, and sediments of the footwall block usually dip very gently beneath the fault plane (reverse drag, type-A flanking structures). Weak normal drag first appears at a slight increase in the dip angle of the main fault in the **Ještěd segment**, having the character of type-B flanking structures. One of the notable elements of footwall-block deformation are bedding-plane slips in the flat-lying Upper Cretaceous sediments. Their occurrences are bound to segments with rather gentle dips of the main fault, which suggests their relation to overthrusting, i.e. to the effects of subhorizontal movement of a block on its immediate footwall.

Steeper dip angles of the main fault in the **Jizera segment** were locally almost perpendicular to the acting compression. Movement of the hangingwall block could have been only partly accommodated by reverse faulting on the main fault, and most of the stress was

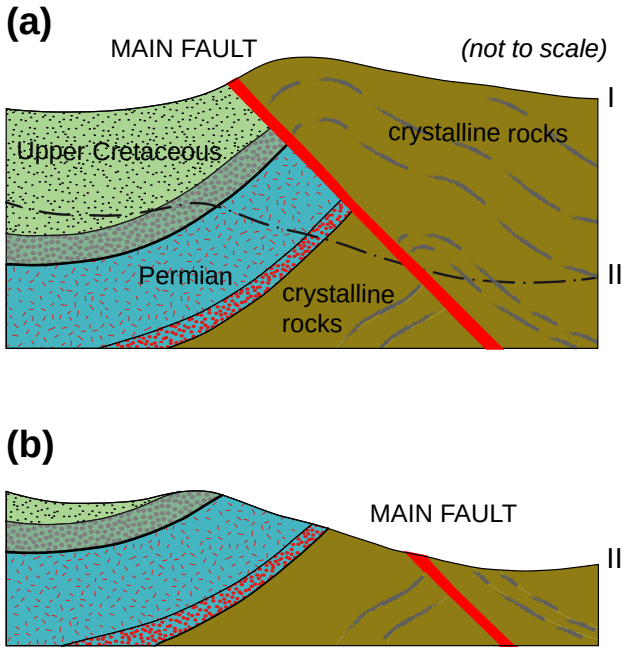

Fig. 19 Low dip angles of the main fault plane modify the traditional view (a) of the position of the Lusatian Fault between the post-Variscan sedimentary basins and the crystalline rocks: the main fault trace may be located inside the crystalline complex in deeper-eroded parts of the fault belt (b). The two different erosional levels are labelled I and II.

transmitted normal to the fault plane to rocks of both blocks at a considerable increase in their loading. This resulted in their "bulldozer-style" deformation (Fig. 20b) with transverse translation of fault-plane segments towards the footwall block. A continuous zone of normal drag structures (type-C and D flanking structures) was formed in the footwall block in the Jizera segment. The intensity of their angular deformation generally increases towards SE alongside with the increase in the dip angle of the main fault. Quartz cementation in the footwall block occurs in a zone hundreds of metres thick, practically coinciding with the drag zone. Such considerable quartz cementation probably resulted from a higher intensity of pressure solution of detrital quartz grains under compression at high angle to the fault plane. The presence of the fault-related ferruginization zone evidences that the main fault functioned as a drainage path for iron-bearing fluids at a certain stage of its history, although its core was partly sealed by fault gouge. Fluid flow along the main fault was also responsible for the origin of barite–fluorite hydrothermal mineralization at Křižany (Horáček et al. 1975). The steep uplift of the hangingwall block was also contributed, besides the movements on the main fault, by internal structures of this block, most notably the numerous reverse faults documented in the Ještěd Crystalline Complex and the drag folds adjacent to the main fault. In the SE part of the Jizera segment, the orientation of the acting stress to the main fault plane was so infavourable that a new fault was formed: the gently dipping Frýdštejn Fault permitted a full relaxation of the acting stress through shear movement. Superposition of the younger pattern of subhorizontally orientated slickensides in the damage zone of the LF is observed at most sites in the Jizera segment.

8. Conclusions

Architecture of the Lusatian Fault (LF), a representative of major Late Cretaceous–Paleogene thrust faults in the foreland of the Alpine–Carpathian deformation front, is described with a clear hierarchical classification of individual architectural elements and their genetic interpretation. The fault core is distinguished within the main fault. In segments with a steeper dip of the main fault, the fault core is delineated by zones of wall-rock brecciation tens of metres thick, representing a structural transition between the fault core and the damage zone of the main fault. Individual elements of the damage zone in the footwall Cretaceous sandstones include deformation

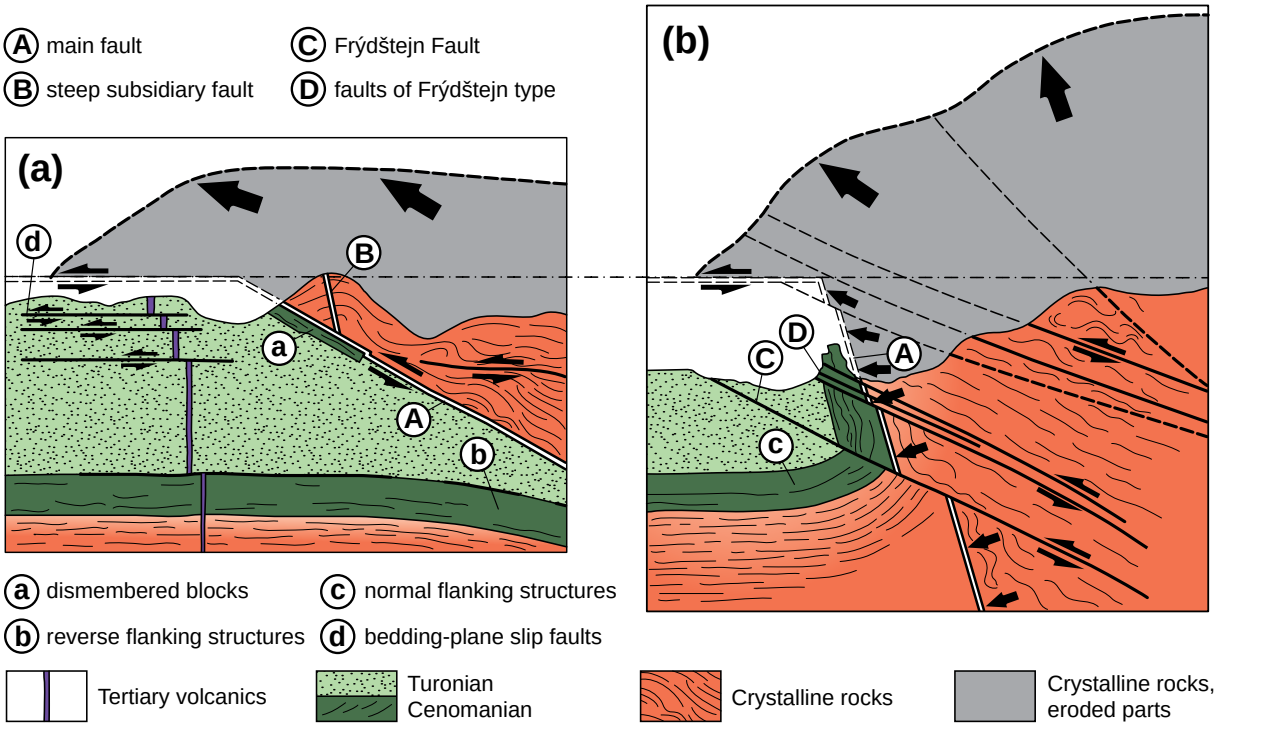

Fig. 20 Two essential architectural styles of the Lusatian Fault Belt, resulting from gently dipping vs. steeply dipping main fault plane. **a –** A flat thrust fault in the Lusatian segment, where the hangingwall block is sheared along the stable-positioned main fault; **b –** A steep thrust fault and a "bulldozer-style" deformation in the Jizera segment, where the large normal component of tectonic stress resulted in transverse translation of fault-plane segments towards the footwall block. This induced additional deformations of pure-shear type in the footwall block, not observed in style (a). Not to scale.

bands, arrays of slickensides, small subsidiary faults and disjunctive cleavage.

A range of structures, brittle or ductile, reach beyond the definition of the damage zone: dismembered blocks, flanking structures, bedding-plane slip faults and accompanying faults (e.g., faults doubling the main fault). They needed not be synchronous with the main thrusting. Early-stage silicification and late-stage ferruginization are also involved. The unit encompassing the LF and these accompanying structures is herein called the Lusatian Fault Belt. We believe that the use of the term "belt" is appropriate for most major thrust faults, especially those with multi-stage kinematic history.

Tectonic style of the LF shows significant alongstrike variations. The Elbsandsteingebirge and the Lusatian segments in the NW are characterized by gentle dip angles of the main fault; the damage zone is narrow (<150 m) and products of tectonic drag are restricted to dismembered blocks of Permian and Jurassic rocks adjacent to the main fault. In contrast, the Jizera segment in the SE is dominated by intermediate to steep dip angles of the main fault. It is characterized by a "bulldozer-style" deformation with a prominent damage zone, a broad zone (490–850 m) of type-C and type-D flanking structures, and doubling of the main fault by a low-angle fault plane. The architecture of the centrally positioned Ještěd segment is transitional between the two types.

Architecture of the whole fault belt and the thicknesses of the individual architectural elements were found to be controlled by the geometry of the main fault under a homogeneous stress (phase $\boldsymbol{\alpha}_1$, NNE–SSW compression; Adamovič and Coubal 1999). The angle between the main fault plane and the acting stress varies among fault segments with different fault-plane orientations. Deformation at these segments therefore shows variable proportions between the pure-shear and simple-shear components; an increase in the pure-shear component implies an increase in the intensity of tectonic drag and in the thicknesses of both the fault core and the damage zone.

Acknowledgments. The paper was produced with the support from the Institutional Research Plan RVO 67985831 of the Institute of Geology AS CR, v.v.i. The early project which covered the first sets of measurements and the excavation of test pits and test trenches was supported by the Czech Science Foundation, project No. 205/96/1754. The authors are indebted to Stanislav Čech for his participation in the documentation of test trenches and suggestions on Cretaceous paleogeography. Ferry Fediuk and Petra Štěpančíková are thanked for the Křižany Mine photo documentation and for the digital elevation model of the fault region, respectively; both provided fruitful discussions over the topic. Martin Šťastný provided identification of mineral phases in fault rocks using X-ray diffraction analysis. All graphics were kindly drawn by Jana Rajlichová. The work of the two anonymous reviewers is greatly appreciated: they not only pointed out the inconsistencies in the text but helped to sharpen the focus of the whole paper. Handling editor Jiří Žák and journal editor Vojtěch Janoušek are thanked for their patience and improvements of the manuscript.

References

Adamovič J, Coubal M (1999) Intrusive geometries and Cenozoic stress history of the northern part of the Bohemian Massif. Geolines 9: 5–14

Adamovič J, Coubal M (2012) Bedding-plane slip movements in Cretaceous sandstones in the Bezděz area. Zpr geol Výzk v Roce 2011: 9–12 (in Czech with English summary)

Bělohradský V, Petrin AV (1977) A Report on Structural–Geological Mapping of the Stráž Block near Křižany and Světlá pod Ještědem 1 : 10 000 in 1976. Unpublished manuscript, archive of the Czech Geological Survey, Prague, pp 1–71 (in Czech)

Bergerat F (1987) Stress fields in the European Platform at the time of Africa–Eurasia collision. Tectonics 6: 99–132

Bergerat F, Angelier J, Andreasson PG (2007) Evolution of paleostress fields and brittle deformation of the Tornquist Zone in Scania (Sweden) during Permo–Mesozoic and Cenozoic times. Tectonophysics 444: 93–110

Braathen A, Tveranger J, Fossen H, Skar T, Cardozo N, Semshaug SE, Bastesen E, Sverdrup E (2009) Fault facies and its application to sandstone reservoirs. AAPG Bulletin 93: 891–917

Brzák P, Fabiánek O, Havránek P (2007) Underground of the Šluknov area and Lužické hory Mts. ZO ČSOP Netopýr, Varnsdorf, pp 1–302 (in Czech)

Caine JS, Bruhn RL, Forster CB (2010) Internal structure, fault rocks, and inferences regarding deformation, fluid flow, and mineralization in the seismogenic Stillwater normal fault, Dixie Valley, Nevada. J Struct Geol 32: 1576–1589

Childs C, Manzocchi T, Walsh JJ, Bonson CG, Nicol A, Schöpfer MPJ (2009) A geometric model of fault zone and fault rock thickness variations. J Struct Geol 31: 117–127

Chrt J (1956) Final Report on Mineral Prospection "Lusatian Fault". Unpublished manuscript, archive of the Czech Geological Survey, Prague, pp 1–16 (in Czech)

Cotta B (1838) Die Lagerungsverhältnisse an der Grenze zwischen Granit und Quader-Sandstein bei Meissen, Hohnstein, Zittau und Liebenau. In: Geognostische Wanderungen II. Arnoldische Buchhandlung, Dresden and Leipzig, pp 1–64

Coubal M (1989) Saxonian Tectogeny in the Central Part of the Bohemian Cretaceous Basin. Unpublished M.Sci.

thesis, Charles University, Prague, pp 1–236 (in Czech)
Coubal M (1990) Compression along faults: example from the Bohemian Cretaceous Basin. Miner Slov 22: 139–144
DEKORP-BASIN Research Group (1999) Deep crustal structure of the northeast German Basin: new DEKORP-BASIN '96 deep profiling results. Geology 27: 55–58
Doležel M (1976) Radial and horizontal fault tectonics in the northern part of the Stráž Block (Cretaceous), Northern Bohemia. Věst Ústř Úst geol 51: 321–329
Faulkner DR, Jackson CAL, Lunn RJ, Schlische RW, Shipton ZK, Wibberley CAJ, Withjack MO (2010) A review of recent developments concerning the structure, mechanics and fluid flow properties of fault zones. J Struct Geol 32: 1557–1575
Fediuk F, Losert J, Röhlich P, Šilar J (1958) Geological setting along the Lusatian Fault in the Šluknov spur. Rozpr Čs Akad Věd, Ř mat přír Věd 9: 1–42 (in Czech)
Fossen H (2010) Structural Geology. Cambridge University Press, New York, pp 1–463
Franzke HJ, Voigt T, von Eynatten H, Brix M, Burmester G (2004) Geometrie and Kinematik der Harznordrandstörung, erläutert an Profilen aus dem Gebiet von Blankenburg. Geowiss Mitt Thüringen 11: 39–62
Horáček J, Chabr P, Syka J (1975) Mining Survey in Structure A-3 and the Origin of Uranium Mineralization at Křižany. Unpublished manuscript, archive of the Czech Geological Survey, Prague, pp 1–117 (in Czech)
Kley J, Voigt T (2008) Late Cretaceous intraplate thrusting in central Europe: effect of Africa–Iberia–Europe convergence, not Alpine collision. Geology 36: 839–842
Kozdrój W, Krentz O, Opletal M (eds) (2001) Comments on the Geological Map Lausitz–Jizera–Karkonosze (without Cenozoic sediments) 1:100 000. Sächsisches Landesamt für Umwelt und Geologie, Freiberg; Państwowy Instytut Geologiczny, Warszawa; Český geologický ústav, Praha, pp 1–64
Krejčí J (1869) Studien im Gebiete der böhmischen Kreide-Formation. I. Vorbemerkungen. Archiv der naturwissenschaftliche Landesdurchforschung von Böhmen. I. Band, Section II. Arbeiten der geologischen Section in den Jahren 1864–1868. Commissions-Verlag bei Fr. Řivnáč, Prag, pp 1–37
Krutský N (1971) Permian along the Lusatian Fault between Rašovka, Světlá p. Ještědem and Jitrava. Čas Mineral Geol 16: 291–300 (in Czech)
Malkovský M (1977) Important faults of the platform cover of the northern part of the Bohemian Massif. Výzk Práce Ústř Úst geol 14: 1–32
Malkovský M (1987) The Mesozoic and Tertiary basins of the Bohemian Massif and their evolution. Tectonophysics 137: 31–42
Mertlík J, Adamovič J (2005) Some significant geomorphic features of the Klokočí Cuesta, Czech Republic. Ferrantia 44: 171–175
Migoń P, Danišík M (2012) Erosional history of the Karkonosze Granite Massif – constraints from adjacent sedimentary basins and thermochronology. Geol Q 56: 441–456
Passchier CW (2001) Flanking structures. J Struct Geol 23: 951–962
Prouza V, Coubal M, Čech S, Málek J (1999) Lusatian Fault. Final Report of the Grant Project GAČR No. 205/96/1754. Unpublished manuscript, archive of the Czech Geological Survey, Prague, pp 1–105 (in Czech)
Prouza V, Coubal M, Adamovič J (2013) Southeastern continuation of the Lusatian Fault in the western Krkonoše Mts. Piedmont region. Zpr geol Výzk v Roce 2012: 59–63 (in Czech with English summary)
Reichmann F (1979) Final Report on Geological Exploration – Křižany. Unpublished manuscript, archive of the Czech Geological Survey, Prague, pp 1–150 (in Czech)
Rousek O, Týlová V (1956) Final Report on Exploration at the Křižany Site. Unpublished manuscript, archive of the Czech Geological Survey, Prague, pp 1–182 (in Czech)
Scheck M, Bayer U, Otto V, Lamarche J, Banka D, Pharaoh T (2002) The Elbe Fault System in North Central Europe – a basement controlled zone of crustal weakness. Tectonophysics 360: 281–299
Sedlář J, Krutský N (1963) Exploration of Limestones and Cement-Producing Minerals, 1959–1962, Ještěd Area. Unpublished manuscript, archive of the Czech Geological Survey, Prague, pp 1–108 (in Czech)
Seifert A (1932) Horizontalverschiebungen im sächsischen Turon-Quader rechts der Elbe als Auswirkungen der Lausitzer Überschiebung. Neu Jb Mineral Geol Paläont, Beil-Bd 69 B: 35–62
Shipton ZK, Soden AM, Kirkpatrick JD, Bright AM, Lunn RJ (2006) How thick is a fault? Fault displacement-thickness scaling revisited. In: Abercrombie R (ed) Earthquakes: Radiated Energy and the Physics of Faulting. Geophysical Monograph Series 170: 193–198
Suess FE (1903) Bau und Bild der Böhmischen Masse. F. Tempsky, G. Freytag, Wien u. Leipzig, pp 1–322
Torabi A, Støren Berg S (2011) Scaling of fault attributes: a review. Mar Petrol Geol 28: 1444–1460
Wagenbreth O (1966) Die Lausitzer Überschiebung und die Geschichte ihrer geologischen Erforschung. I. Abh Staatl Mus Mineral Geol (Dresden) 11: 163–279
Wagenbreth O (1967) Die Lausitzer Überschiebung und die Geschichte ihrer geologischen Erforschung. II. Abh Staatl Mus Mineral Geol (Dresden) 12: 279–368
Weiss CS (1827) Über einige geognostische Punkte bei Meissen und Hohenstein. Karstens Arch Bergb u. Hüttenwes (Berlin) 16: 3–16
Woodcock NH, Mort K (2008) Classification of fault breccias and related fault rocks. Geol Mag 145: 435–400
Zahálka Č (1902) Formation I of the Cretaceous period in the Jizera River Basin. Věst Král Čes Společ Nauk, Tř math-přírodověd 3: 1–15 (in Czech)

Ziegler PA (1987) Late Cretaceous and Cenozoic intra-plate compressional deformations in the Alpine foreland – a geodynamic model. Tectonophysics 137: 389–420

Ziegler PA, Dèzes P (2007) Cenozoic uplift of Variscan massifs in the Alpine foreland: timing and controlling mechanisms. Global Planet Change 58: 237–269